

A Discontinuous Galerkin and Semismooth Newton Approach for the Numerical Solution of the Nonhomogeneous Bingham Flow*

Sergio González-Andrade

Research Center on Mathematical Modeling (MODEMAT) and
Departamento de Matemática - Escuela Politécnica Nacional
Ladrón de Guevara E11-253, Quito 170413, Ecuador
`sergio.gonzalez@epn.edu.ec`

Paul E. Méndez Silva

Research Center on Mathematical Modeling (MODEMAT) - Escuela Politécnica Nacional
Ladrón de Guevara E11-253, Quito 170413, Ecuador
`paul.mendez01@epn.edu.ec`

January 27, 2022

Abstract

This paper is devoted to the study of non-homogeneous Bingham flows. We introduce a second-order, divergence-conforming discretization for the Bingham constitutive equations, coupled with a discontinuous Galerkin scheme for the mass density. One of the main challenges when analyzing viscoplastic materials is the treatment of the yield stress. In order to overcome this issue, in this work we propose a local regularization, based on a Huber smoothing step. We also take advantage of the properties of the divergence conforming and discontinuous Galerkin formulations to incorporate upwind discretizations to stabilize the formulation. The stability of the continuous problem and the full-discrete scheme are analyzed. Further, a semismooth Newton method is proposed for solving the obtained fully-discretized system of equations at each time step. Finally, several numerical examples that illustrate the main features of the problem and the properties of the numerical scheme are presented.

Keywords: Bingham fluids, discontinuous-Galerkin method, semismooth Newton methods.

AMS Subject Classification: 76A05. 76-10. 65M60. 49M15.

1 Introduction

1.1 Scope

We are interested in the analysis and numerical approximation of the nonhomogeneous Bingham flow. The governing equations for this process can be formulated as follows. Given a bounded connected domain Ω in \mathbb{R}^d , $d = 2$ or 3 , with a Lipschitz-continuous boundary and a positive

*Supported in part by the Escuela Politécnica Nacional del Ecuador, under the project PIS 18-03.

real number T , the following system of partial differential equations describes a non homogeneous unsteady Bingham flow

$$\begin{aligned} \partial_t \rho + \mathbf{u} \cdot \nabla \rho &= 0, & \text{in } \Omega \times]0, T[, \\ \rho \partial_t \mathbf{u} + \rho(\mathbf{u} \cdot \nabla) \mathbf{u} - \text{Div } \boldsymbol{\tau} + \nabla p &= \mathbf{f}, & \text{in } \Omega \times]0, T[, \\ \text{div } \mathbf{u} &= 0, & \text{in } \Omega \times]0, T[, \end{aligned} \tag{1}$$

where the fluid stress tensor $\boldsymbol{\tau}$ is

$$\begin{cases} \boldsymbol{\tau} = 2\mu \mathbf{D}\mathbf{u} + \tau_s \frac{\mathbf{D}\mathbf{u}}{|\mathbf{D}\mathbf{u}|} & \text{if } \mathbf{D}\mathbf{u} \neq 0, \\ |\boldsymbol{\tau}| \leq \tau_s & \text{if } \mathbf{D}\mathbf{u} = 0, \end{cases}$$

and the sought quantities are the density ρ , the velocity of the fluid \mathbf{u} , and the pressure p . We endow the problem with appropriate initial data

$$\rho(0) = \rho_0, \mathbf{u}(0) = \mathbf{0} \quad \text{in } \Omega \times \{0\},$$

and boundary conditions in the following manner:

$$\begin{aligned} \rho(\mathbf{x}, t) &= \psi(\mathbf{x}, t), & (\mathbf{x}, t) \text{ in } \Gamma_{\text{in}} \times]0, T[, \\ \mathbf{u}(\mathbf{x}, t) &= \mathbf{g}(\mathbf{x}, t), & (\mathbf{x}, t) \text{ in } \Gamma \times]0, T[. \end{aligned}$$

Bingham is the seminal model for viscoplastic fluids, which are materials with rheology defined by a yield stress τ_s . This rheological characteristic implies that the material hardens in regions where the stress do not exceed the yield stress. Meanwhile, in the regions where the stress exceeds this value τ_s , the material flows as a viscous fluid with a plastic behavior. Because of this mechanical property, one particularity of Bingham models is the presence of rigid moving parts in the interior of the flow. The size and location of this rigid zones depends on the yield stress, and can even block the flow for high values of this parameter. This so called *blocking property* makes the study of these materials of interest in various fields and applications. For instance, when related to the flow of biological fluids, such as blood or mucus, a blocking could be an indicator of a health compromising phenomena (see [10]).

For a nonhomogeneous Bingham model we have to consider, as shown in (1), a coupled system between a Navier-Stokes type equation and a first order transport equation modelling the changing density. This makes the problem challenging from the PDEs theory perspective. For the mathematical theory on the well posedness of problem (1), we refer to [4, 7, 12, 30]. Particularly, in [7], the author analyses a variational formulation for the nonhomogeneous Bingham flow, by using the classical variational inequality approach, and proves the existence of weak solutions for (1). Further, the author finds regularity conditions to obtain uniqueness of solutions. In this work, we focus on the numerical simulation of this flow problem, considering that the theoretical results hold.

For developing numerical approximations to this problem, it seems natural to look at the techniques established for the solution of constant density incompressible Navier-Stokes equations, and try to exploit them, as far as possible. It is the purpose of this paper to advance a second-order divergence-conforming discretization for this problem. Specifically, we introduce an $\mathbf{H}(\text{div})$ -conforming method based on Brezzi-Douglas-Marini (BDM) spaces [8], coupled with a discontinuous Galerkin discretization for density, both equations stabilized with upwind terms as in [11, 15] and combined with an implicit, second-order backward differentiation formula (BDF2) for time discretization.

Between the exactly divergence-free methods advantages we can mention: First, they are pressure-robust, which means, it is possible to separate velocity and pressure completely in the error analysis. Also, using an $\mathbf{H}(\text{div})$ -conforming FEM allows the usage of discontinuous Galerkin Finite element method (dG-FEM) techniques in the analysis of the formulation and the treatment of the convective term. In fact, an upwind discretization can be incorporated quite naturally, which allows to obtain Reynolds-semi-robust estimates. Moreover, the fact that less stability is required implies that the amount of numerical dissipation added is minimized. Finally, the conservation properties of the exact conservation equations of mass, energy and momentum are naturally transferred to the discrete solution [31].

1.2 Related Work

While there is a rich body of literature on numerical approximation of the constant density and viscosity Navier–Stokes equations, fewer results are available for the non-homogeneous case. Numerical approximation to similar coupled flow systems were studied with many different numerical methods, including projection methods [29, 22], fractional-step methods [17, 23], and the discontinuous Galerkin (dG) method [28]. Furthermore, the numerical simulation of the variable density incompressible Navier-Stokes system was studied in [9], where the authors introduce an hybrid scheme which combines a Finite Volume approach for treating the mass conservation equation and a Finite Element method to deal with the momentum equation and the divergence free constraint.

The $\mathbf{H}(\text{div})$ -conforming approach for the Brinkman equation was studied numerically by [27], while exactly divergence-free $\mathbf{H}(\text{div})$ -conforming finite element methods for time-dependent incompressible viscous flow problems have been extensively studied by [31], with special emphasis on pressure and Reynolds semi-robustness of the formulations.

In the case of nonhomogeneous or density-dependent Bingham flow, mixing and interaction of materials with different densities are a mainly interesting field for the engineering and mathematical communities. For instance, several contributions have discussed this model as a suitable background for landslides and, in general, for debris flows (see [24, 25]). This assertion comes from the fact that debris flows are flows involving several substances including mixtures and suspensions of granular particles in water, sand and organic mass, among others. These substances, depending on the physical conditions, can create rigid zones moving in the flow, casting the expected behaviour of a viscoplastic Bingham material. Further, the flow is not expected to be homogeneous, since the density varies depending on the concentration of the component substances.

One interesting and challenging problem is the so called Rayleigh–Taylor instability when two fluids interact. In [14] and [16], the authors analyse this phenomenon for two viscoplastic materials by using a volume of fluid (VOF) method and a hydrodynamic simulation based on the Bingham model. Further, in [5], among other contributions, the authors perform an experimental study of the behaviour of viscoplastic drops moving in a given media, usually with different densities. In contrast with most of these contributions, in this paper, we are focused on the numerical simulation of this phenomena, based on the variational analysis of the constitutive PDEs for the nonhomogeneous Bingham flow.

1.3 Outline of the paper

The remainder of this paper is organized as follows. In Section 2, we introduce the continuous formulation of problem 1 and recall its main properties. We also propose and briefly analyze the local Huber regularization for the problem. In Section 3, we describe the time semi-discretization, and then the complete discrete scheme of this problem, briefly addressing stability properties. We

also discuss the semismooth Newton linearization of each time step. Finally, in Section 4, we illustrate the properties of the problem and the scheme with numerical examples generated by the method introduced. We close the paper with some remarks and discussions given in Section 5.

2 The continuous formulation

In this section we introduce and analyze a transient formulation of the coupled problem. We start by introducing some notation. We denote by $L^p(\Omega)$ and $W^{r,p}(\Omega)$ the usual Lebesgue and Sobolev spaces with respective norms $\|\cdot\|_{L^p(\Omega)}$ and $\|\cdot\|_{W^{r,p}(\Omega)}$. If $p = 2$ we write $H^r(\Omega)$ and $\|\cdot\|_{r,\Omega}$ in place of $W^{r,p}(\Omega)$ and $\|\cdot\|_{W^{r,p}(\Omega)}$. By \mathbf{L} and \mathbb{L} we denote the corresponding vectorial and tensorial counterparts of the scalar functional space L , respectively. Further, we denote by $(\cdot, \cdot)_\Omega$ the usual inner product in $L^2(\Omega)$. Moreover, for any vector field $\mathbf{v} = (v_i)_{i=1,d}$ we set the gradient, symmetric part of the gradient and divergence, as

$$\nabla \mathbf{v} := \left(\frac{\partial v_i}{\partial x_j} \right)_{i,j=1,d}, \quad \mathbf{D}\mathbf{v} := \frac{1}{2} (\nabla \mathbf{v} + (\nabla \mathbf{v})^T) \quad \text{and} \quad \operatorname{div} \mathbf{v} := \sum_{j=1}^d \frac{\partial v_j}{\partial x_j},$$

respectively, and we use the vector-valued Hilbert spaces

$$\begin{aligned} \mathbf{H}(\operatorname{div}; \Omega) &:= \{ \mathbf{w} \in \mathbf{L}^2(\Omega) : \operatorname{div} \mathbf{w} \in L^2(\Omega) \}, \\ \mathbf{H}_0(\operatorname{div}; \Omega) &:= \{ \mathbf{w} \in \mathbf{H}(\operatorname{div}; \Omega) : \mathbf{w} \cdot \mathbf{n}_{\partial\Omega} = 0 \text{ on } \partial\Omega \}, \\ \mathbf{H}_0(\operatorname{div}^0; \Omega) &:= \{ \mathbf{w} \in \mathbf{H}_0(\operatorname{div}; \Omega) : \operatorname{div} \mathbf{w} = 0 \text{ in } \Omega \}, \end{aligned}$$

where $\mathbf{n}_{\partial\Omega}$ denotes the outward normal on $\partial\Omega$. For a given tensor \mathcal{T} , we let $\operatorname{Div} \mathcal{T}$ be the divergence operator acting along the rows of \mathcal{T} . We denote by $L^s(0, T; W^{m,p}(\Omega))$ the Banach space of all L^s -integrable functions from $[0, T]$ into $W^{m,p}(\Omega)$, with norm

$$\|v\|_{L^s(0,T;W^{m,p}(\Omega))} = \begin{cases} \left(\int_0^T \|v(t)\|_{W^{m,p}(\Omega)}^s dt \right)^{1/s} & \text{if } 1 \leq s < \infty, \\ \operatorname{ess\,sup}_{t \in [0,T]} \|v(t)\|_{W^{m,p}(\Omega)} & \text{if } s = \infty. \end{cases}$$

2.1 Huber regularization

The main characteristic of viscoplastic materials is the existence of a yield stress. In fact, these fluids exhibit a non-Newtonian behaviour depending on this parameter: if the total stress is below the yield stress, the fluid moves without continuous deformation, which means that the material is at rest or is moving as a rigid solid. On the other hand, if the stress overpasses the yield stress, the fluid flows with continuous deformation. In the particular case of the Bingham model, in the regions where the material flows, the expected behaviour corresponds to a Newtonian fluid.

The complex behaviour of Bingham fluids is given in the model by the proposed structure of the stress:

$$\begin{cases} \boldsymbol{\tau} = 2\mu \mathbf{D}\mathbf{u} + \tau_s \frac{\mathbf{D}\mathbf{u}}{|\mathbf{D}\mathbf{u}|}, & \text{if } \mathbf{D}\mathbf{u} \neq 0 \\ |\boldsymbol{\tau}| \leq \tau_s, & \text{if } \mathbf{D}\mathbf{u} = 0. \end{cases} \quad (2)$$

Note that in the so called yielded regions, *i.e.*, regions where $\mathbf{D}\mathbf{u} \neq 0$, the stress is given as a sum of two terms: a viscous term, associated to the viscosity μ , and a plastic term associated with the yield stress τ_s . Furthermore, in the unyielded regions, where $\mathbf{D}\mathbf{u} = 0$, we only know that the stress is bounded. This is the main issue regarding the mathematical modelling and the numerical

solution of these materials: in general, we do not have an a priori knowledge about the localization of the yielded or unyielded regions in the flow. Because of this fact, we are dealing with an ill-posed problem.

One classical approach for the analysis and numerical solution of these materials is to regularize the stress tensor. In this work we propose a local regularization, based on a Huber smoothing step, which applied to (2), reads as follows:

$$\boldsymbol{\tau}_\gamma := 2\mu\mathbf{D}\mathbf{u} + \tau_s\gamma \frac{\mathbf{D}\mathbf{u}}{|\mathbf{D}\mathbf{u}|_\gamma}, \quad (3)$$

where $|\boldsymbol{\tau}|_\gamma := \max\{\tau_s, \gamma|\boldsymbol{\tau}|\}$. Here $\gamma \gg 0$ is a given regularization parameter, expected to be as big as possible. This is a local regularization approach, which has proven to be efficient and reliable for the numerical solution of several viscoplastic flow problems (see [13, 20]).

The main advantage of the Huber regularization is that it is a local procedure which is designed to preserve, qualitatively, the structure of the model in the whole geometry. Due to this fact, the smoothing approach allows us to directly define regions that approximate the yielded and unyielded regions in the flow in the following manner: the yielded regions are approximated by regions where $|\mathbf{D}\mathbf{u}| \geq \frac{\tau_s}{\gamma}$, while the unyielded regions are approximated by regions where $|\mathbf{D}\mathbf{u}| < \frac{\tau_s}{\gamma}$. One of the main characteristic of the flow is the fact that the viscosity of the material is supposed to jump to infinity when crossing the separating phase from the yielded to the unyielded regions (let us recall that the model understands that the material moves like a rigid solid in the unyielded regions). Considering that the parameter γ needs to be large enough, the smoothing procedure sets a large viscosity in the unyielded regions and the actual viscosity of the material in the yielded regions. Because of this fact, the approach is usually known as a bi-viscosity regularization ([6]).

Summarizing, the system of Huber regularized constitutive equations for the non-homogeneous Bingham flow is given by

$$\begin{aligned} \partial_t \rho + \mathbf{u} \cdot \nabla \rho &= 0, & \text{in } \Omega \times]0, T[, \\ \rho \partial_t \mathbf{u} + \rho(\mathbf{u} \cdot \nabla) \mathbf{u} - \text{Div } \boldsymbol{\tau}_\gamma + \nabla p &= \mathbf{f}, & \text{in } \Omega \times]0, T[, \\ \text{div } \mathbf{u} &= 0, & \text{in } \Omega \times]0, T[, \\ \boldsymbol{\tau}_\gamma &:= 2\mu\mathbf{D}\mathbf{u} + \tau_s\gamma \frac{\mathbf{D}\mathbf{u}}{|\mathbf{D}\mathbf{u}|_\gamma}, & \text{a.e. in } \Omega \times]0, T[\end{aligned} \quad (4)$$

2.2 Weak formulation

Let us define the following spaces

$$\begin{aligned} \mathbf{V} &:= \mathbf{H}_0^1(\Omega), \quad \mathcal{Q} := L_0^2(\Omega), \quad \mathcal{W} := H_0^1(\Omega), \\ \mathbf{V}^t &:= \{\mathbf{w} \in \mathbf{L}^2(0, T; \mathbf{V}) : \partial_t \mathbf{w} \in L^2(0, T; \mathbf{L}^2(\Omega))\}, \\ \mathcal{Q}^t &:= L^2(0, T; \mathcal{Q}), \\ \mathcal{W}^t &:= \{s \in L^2(0, T; \mathcal{W}) : \partial_t s \in L^2(0, T; L^2(\Omega))\}. \end{aligned}$$

Testing each equation in problem (4) against suitable functions and integrating by parts whenever adequate, gives the following weak formulation: Find $(\rho, \mathbf{u}, p) \in \mathcal{W}^t \times \mathbf{V}^t \times \mathcal{Q}^t$ such that for

all $(\zeta, \mathbf{v}, q) \in \mathcal{W} \times \mathbf{V} \times \mathcal{Q}$ and for a.e. $t \in [0, T]$,

$$\begin{aligned} \int_{\Omega} \partial_t \rho \zeta \, dx + c_1(\mathbf{u}, \rho, \zeta) &= 0, \\ \int_{\Omega} \rho \partial_t \mathbf{u} \cdot \mathbf{v} \, dx + a_2(\mathbf{u}, \mathbf{v}) + c_2(\rho, \mathbf{u}; \mathbf{u}, \mathbf{v}) + b(\mathbf{v}, p) &= \int_{\Omega} \mathbf{f} \cdot \mathbf{v} \, dx, \\ b(\mathbf{u}, q) &= 0, \end{aligned} \tag{5}$$

where the variational forms $a_2 : \mathbf{V} \times \mathbf{V} \rightarrow \mathbb{R}$, $c_2 : \mathcal{W} \times \mathbf{V} \times \mathbf{V} \rightarrow \mathbb{R}$, $c_1 : \mathbf{V} \times \mathcal{W} \times \mathcal{W} \rightarrow \mathbb{R}$ and $b : \mathbf{V} \times \mathcal{Q} \rightarrow \mathbb{R}$ are defined as follows, for all $\mathbf{u}, \mathbf{v}, \mathbf{w} \in \mathbf{V}$, $q \in \mathcal{Q}$, $\rho, \zeta \in \mathcal{W}$:

$$\begin{aligned} a_2(\mathbf{u}, \mathbf{v}) &:= \int_{\Omega} (\mu \mathbf{D}\mathbf{u} : \mathbf{D}\mathbf{v}) \, dx + \int_{\Omega} \frac{\tau_s \gamma}{|\mathbf{D}\mathbf{u}|_{\gamma}} \mathbf{D}\mathbf{u} : \mathbf{D}\mathbf{v} \, dx, \\ c_2(\rho \mathbf{w}; \mathbf{u}, \mathbf{v}) &:= \int_{\Omega} (\rho \mathbf{w} \cdot \nabla) \mathbf{u} \cdot \mathbf{v} \, dx + \frac{1}{2} \int_{\Omega} \nabla \cdot (\rho \mathbf{w}) \mathbf{u} \cdot \mathbf{v} \, dx, \\ c_1(\mathbf{u}; \rho, \zeta) &:= \int_{\Omega} (\mathbf{u} \cdot \nabla \rho) \zeta \, dx, \\ b(\mathbf{u}, q) &= - \int_{\Omega} q \operatorname{div} \mathbf{u} \, dx. \end{aligned}$$

Note that we use a common consistent skew symmetric form of operator $c_2(\cdot; \cdot, \cdot)$. This alternative form of the momentum equation will preserve exactly the kinetic energy balance at the discrete level without invoking mass conservation (see for instance [22]).

2.3 Stability of the continuous problem

For the sake of simplicity, we will use homogeneous Dirichlet boundary condition for velocity in our analysis. Note that more general boundary conditions can still be handled by similar techniques (see, e.g., [22]). It is also worth noticing that, for a homogeneous Dirichlet condition on the normal component of the velocity on the entire $\partial\Omega$, no boundary condition needs to be specified for the density.

First we recall that the Sobolev embedding Theorem (for instance as in [1]) establishes the continuous injection $i_r : H^r(\Omega) \rightarrow L^{2p}(\Omega)$, where

$$2p = \begin{cases} \frac{1}{1-r} & \text{if } d = 2, \\ \frac{6}{3-2r} & \text{if } d = 3, \end{cases}$$

and there holds,

$$\|v\|_{L^{2p}(\Omega)} \leq C_r \|v\|_{r,\Omega} \text{ for all } v \in H^r(\Omega). \tag{6}$$

Now we apply the Cauchy-Schwarz and Hölder inequalities, and (6) to prove that the variational forms defined above are continuous for all $\mathbf{u}, \mathbf{v}, \mathbf{w} \in \mathbf{V}$, $q \in \mathcal{Q}$, and $\rho, \zeta \in \mathcal{W}$:

$$|a_2(\mathbf{u}, \mathbf{v})| \leq C_a \|\mathbf{u}\|_{1,\Omega} \|\mathbf{v}\|_{1,\Omega}, \tag{7a}$$

$$|b(\mathbf{v}, q)| \leq C_b \|\mathbf{v}\|_{1,\Omega} \|q\|_{0,\Omega}, \tag{7b}$$

$$|c_2(\rho \mathbf{w}; \mathbf{u}, \mathbf{v})| \leq C_c \|\rho\|_{1,\Omega} \|\mathbf{w}\|_{1,\Omega} \|\mathbf{u}\|_{1,\Omega} \|\mathbf{v}\|_{1,\Omega}, \tag{7c}$$

$$|c_1(\mathbf{u}; \rho, \zeta)| \leq \hat{C}_c \|\mathbf{u}\|_{1,\Omega} \|\rho\|_{1,\Omega} \|\zeta\|_{1,\Omega}. \tag{7d}$$

We also recall (from [19, Chapter I, Lemma 3.1], for instance) the following Poincaré-Friedrichs inequality:

$$\|\varphi\|_{0,\Omega} \leq C_p |\varphi|_{1,\Omega}, \quad \text{for all } \varphi \in H_0^1(\Omega). \quad (8)$$

Next, we consider the bilinear form $a_2(\cdot, \cdot)$. Note that, for $\mathbf{v} \in \mathbf{H}_0^1(\Omega)$, we have that

$$\begin{aligned} a_2(\mathbf{v}, \mathbf{v}) &= \mu \int_{\Omega} |\mathbf{D}\mathbf{v}|^2 dx + \gamma \tau_s \int_{\Omega} \frac{|\mathbf{D}\mathbf{v}|^2}{|\mathbf{D}\mathbf{v}|_\gamma} dx \\ &\geq C \|\mathbf{D}\mathbf{v}\|_{0,\Omega}^2 dx. \end{aligned}$$

Hence, Korn's inequality and inequality (8) readily gives the coercivity of a_2 , i.e., there exist a positive constant α_a such that

$$a_2(\mathbf{v}, \mathbf{v}) \geq \alpha_a \|\mathbf{v}\|_{1,\Omega}^2, \quad \text{for all } \mathbf{v} \in \mathbf{H}_0^1(\Omega). \quad (9a)$$

Using the definition and characterisation of the kernel of the bilinear form $b(\cdot, \cdot)$, we can write

$$\mathbf{K} := \{\mathbf{v} \in \mathbf{H}_0^1(\Omega) : b(\mathbf{v}, q) = 0, \quad \forall q \in L_0^2(\Omega)\} = \{\mathbf{v} \in \mathbf{H}_0^1(\Omega) : \operatorname{div} \mathbf{v} = 0 \text{ in } \Omega\},$$

and applying integration by parts, we can readily observe that (see [22, Lemma 1], also [29])

$$c_2(\rho \mathbf{w}; \mathbf{v}, \mathbf{v}) = 0 \quad \text{and} \quad c_1(\mathbf{w}; \rho, \rho) = 0, \quad \text{for all } \mathbf{w} \in \mathbf{K}, \mathbf{v} \in \mathbf{H}^1(\Omega), \rho \in H^1(\Omega). \quad (10)$$

It is well known that the bilinear form $b(\cdot, \cdot)$ satisfies the inf-sup condition (see, e.g., [32]):

$$\sup_{\mathbf{v} \in \mathbf{H}_0^1(\Omega) \setminus \{0\}} \frac{b(\mathbf{v}, q)}{\|\mathbf{v}\|_{1,\Omega}} \geq \beta \|q\|_{0,\Omega}, \quad \text{for all } q \in L_0^2(\Omega).$$

Lemma 2.1 (Stability). *If $\mathbf{f} \in L^\infty(0, T; \mathbf{L}^2(\Omega))$, $\mathbf{u}_0 \in \mathbf{L}^2(\Omega)$ and $\rho_0 \in L^2(\Omega)$, then, for any solution (\mathbf{u}, ρ) of (5) and for $t \in (0, T]$, there exists a constant $C > 0$ such that*

$$\|\sqrt{\rho} \mathbf{u}\|_{L^2(0,t; \mathbf{H}^1(\Omega))} + \|\rho\|_{L^2(0,t; H^1(\Omega))} \leq C (\|\sqrt{\rho_0} \mathbf{u}_0\|_{0,\Omega} + \|\rho_0\|_{0,\Omega} + \|\mathbf{f}\|_{L^\infty(0,T; \mathbf{L}^2(\Omega))}),$$

Proof. First taking $\zeta = \rho$, in the first equation of (5) and using (10), we obtain the following identity:

$$\frac{1}{2} \frac{d}{dt} \|\rho\|_{0,\Omega}^2 = 0$$

Integrating this equation between 0 and t yields, in particular that

$$\|\rho(\cdot, t)\|_{0,\Omega} \leq \|\rho_0\|_{0,\Omega}. \quad (11)$$

Now, we can take \mathbf{u} on \mathbf{K} and due to the inf-sup condition we can solve an equivalent reduced problem where $b(\cdot, \cdot)$ is removed from the variational form (5). Setting $\mathbf{v} = \mathbf{u}$ and using (10) and (9a), we have

$$\frac{1}{2} \frac{d}{dt} \|\sqrt{\rho} \mathbf{u}\|_{0,\Omega}^2 + \alpha_a \|\mathbf{u}\|_{1,\Omega}^2 \leq \|\mathbf{f}\|_{0,\Omega} \|\mathbf{u}\|_{0,\Omega}.$$

Now we use Young's inequality with $\varepsilon = \alpha_a/4$ to get

$$\frac{1}{2} \frac{d}{dt} \|\sqrt{\rho} \mathbf{u}\|_{0,\Omega}^2 + \frac{\alpha_a}{2} \|\mathbf{u}\|_{1,\Omega}^2 \leq C \|\mathbf{f}\|_{0,\Omega}^2$$

Analogously, after integrating from 0 to t we find that

$$\|\sqrt{\rho} \mathbf{u}(\cdot, t)\|_{0,\Omega} + \alpha_a \int_0^t \|\mathbf{u}(\cdot, z)\|_{1,\Omega}^2 dz \leq \|\sqrt{\rho_0} \mathbf{u}_0\|_{0,\Omega} + C \int_0^t \|\mathbf{f}\|_{0,\Omega}^2 dz \quad (12)$$

Finally, we derive the sought result from (11) and (12). \square

3 The discrete formulation

In this section we introduce the Galerkin scheme associated with problem (5).

3.1 The time semi-discrete problem

In order to describe the time discretization of equation (1), we introduce a partition of the interval $[0, T]$ into subintervals $[t_{n-1}, t_n]$, $1 \leq n \leq N$, such that $0 = t_0 < t_1 < \dots < t_N = T$. We use the implicit BDF2 scheme, where all first-order time derivatives are approximated using the centered operator

$$\partial_t \mathbf{u}(t_{n+1}) \approx \frac{1}{\Delta t} \left(\frac{3}{2} \mathbf{u}^{n+1} - 2\mathbf{u}^n + \frac{1}{2} \mathbf{u}^{n-1} \right), \quad (13)$$

(similarly for $\partial_t \rho$), and for the first time step a first-order backward Euler method is used from t^0 to t^1 , starting from the interpolates \mathbf{u}^0 and ρ^0 of the initial data.

In what follows, we define the difference operator

$$\mathcal{D}y^{n+1} := 3y^{n+1} - 4y^n + y^{n-1},$$

for any quantity indexed by the time step n . For instance, (13) can be written as $\partial_t \mathbf{u}(t_{n+1}) \approx \frac{1}{2\Delta t} \mathcal{D}\mathbf{u}^{n+1}$.

In the following sections, we discuss a dG discretization for the space variables, and present the fully discretized system to be solved by a semismooth Newton iteration.

3.2 A Divergence-conforming-dG FEM coupled scheme

Let $\{\mathcal{T}_h\}_{h>0}$ be a regular family of triangulations of Ω by simplices K (triangles in \mathbb{R}^2 and tetrahedra in \mathbb{R}^3 respectively), and set $h := \max\{h_K : K \in \mathcal{T}_h\}$. We label by K^- and K^+ the two elements adjacent to a facet e (an edge in 2D or a face in 3D). Let \mathcal{E}_h denote the set of all facets and $\mathcal{E}_h = \mathcal{E}_h^i \cup \mathcal{E}_h^\partial$ where \mathcal{E}_h^i and \mathcal{E}_h^∂ are the subset of interior facets and boundary facets, respectively. If \mathbf{v} and w are a smooth vector and a scalar field defined on $\{\mathcal{T}_h\}$, then (\mathbf{v}^\pm, w^\pm) denote the traces of (\mathbf{v}, w) on e that are the extensions from the interior of K^+ and K^- , respectively. Let \mathbf{n}_e denote the outward unit normal vector to e on K . The average $\{\{\cdot\}\}$ and jump $\llbracket \cdot \rrbracket$ operators are defined as

$$\{\{\mathbf{v}\}\} := (\mathbf{v}^- + \mathbf{v}^+)/2, \quad \{\{w\}\} := (w^- + w^+)/2, \quad \llbracket \mathbf{v} \rrbracket := (\mathbf{v}^- - \mathbf{v}^+), \quad \llbracket w \rrbracket := (w^- - w^+),$$

whereas, for boundary jumps and averages, we adopt the conventions $\{\{\mathbf{v}\}\} = \llbracket \mathbf{v} \rrbracket = \mathbf{v}$, and $\{\{w\}\} = \llbracket w \rrbracket = w$. Moreover, \mathbf{D}_h will denote the broken analogous of operator \mathbf{D} .

For $k \geq 1$, consider the following finite element subspaces:

$$\begin{aligned} \mathbf{V}_h &:= \{ \mathbf{v}_h \in \mathbf{H}(\text{Div}; \Omega) : \mathbf{v}_h|_K \in [\mathbb{P}^k(K)]^d \quad \forall K \in \mathcal{T}_h \}, \\ \mathcal{Q}_h &:= \{ q_h \in L_0^2(\Omega) : q_h|_K \in \mathbb{P}^{k-1}(K) \quad \forall K \in \mathcal{T}_h \}, \\ \mathcal{W}_h &:= \{ s_h \in L^2(\Omega) : s_h|_K \in \mathbb{P}^{k-1}(K) \quad \forall K \in \mathcal{T}_h \}, \\ \mathbf{W}_h &:= \left\{ \mathbf{w} \in \mathbb{L}^2(\Omega) : \mathbf{w}|_K \in [\mathbb{P}^{k-1}(K)]^{d \times d}, \quad \forall K \in \mathcal{T}_h \right\}, \end{aligned}$$

Associated with these finite-dimensional spaces, we state the following semi-discrete Galerkin formulation: Find $(\rho_h, \mathbf{u}_h, p_h, \mathbf{z}_h) \in \mathcal{W}_h \times \mathbf{V}_h \times \mathcal{Q}_h \times \mathbf{W}_h$, such that, for all $(\mathbf{v}_h, q_h, \zeta_h, \mathbf{w}_h) \in$

$$\mathbf{V}_h \times \mathcal{Q}_h \times \mathcal{W}_h \times \mathbf{W}_h:$$

$$\begin{aligned} (\partial_t \rho_h, \zeta_h)_\Omega + c_1^h(\mathbf{u}_h, \rho_h, \zeta_h) &= 0 \\ (\sigma_h \partial_t(\sigma_h \mathbf{u}_h), \mathbf{v}_h)_\Omega + a_2^h(\mathbf{u}_h, \mathbf{v}_h) + (\mathbf{z}_h, \mathbf{D}_h \mathbf{v}_h)_\Omega + c_2^h(\rho_h \mathbf{u}_h; \mathbf{u}_h, \mathbf{v}_h) + b(p_h, \mathbf{v}_h) &= \int_\Omega \mathbf{f} \cdot \mathbf{v}_h \, dx, \\ b(q_h, \mathbf{u}_h) &= 0 \\ (\gamma \tau_s \mathbf{D}_h \mathbf{u}_h)_\Omega - (|\mathbf{D}_h \mathbf{u}_h|_\gamma \mathbf{z}_h, \mathbf{w}_h)_\Omega &= 0. \end{aligned} \quad (14)$$

Here $\sigma_h = \sqrt{\rho_h}$, and the discrete versions of the forms $a_2^h(\cdot, \cdot)$, $c_2^h(\cdot, \cdot; \cdot, \cdot)$ and $c_1^h(\cdot; \cdot, \cdot)$ are defined using a symmetric interior penalty approach in the first case and upwind approach for the two convective terms:

$$a_2^h(\mathbf{u}_h, \mathbf{v}_h) := \int_\Omega (\mu \mathbf{D}_h \mathbf{u}_h : \mathbf{D}_h \mathbf{v}_h) \, dx \quad (15)$$

$$+ \sum_{e \in \mathcal{E}_h} \int_e \left(-\{\{\mu \mathbf{D}_h(\mathbf{u}_h) \mathbf{n}_e\}\} \cdot \llbracket \mathbf{v}_h \rrbracket - \{\{\mu \mathbf{D}_h(\mathbf{v}_h) \mathbf{n}_e\}\} \cdot \llbracket \mathbf{u}_h \rrbracket + \frac{a_0}{h_e} \mu \llbracket \mathbf{u}_h \rrbracket : \llbracket \mathbf{v}_h \rrbracket \right) \, ds, \quad (16)$$

$$c_1^h(\mathbf{u}_h; \rho_h, \zeta_h) := \int_\Omega (\mathbf{u}_h \cdot \nabla \rho_h) \zeta_h \, dx - \sum_{e \in \mathcal{E}_h} \int_e (\mathbf{u}_h \cdot \mathbf{n}_e) \llbracket \rho_h \rrbracket \{\{\zeta_h\}\} \, ds \quad (17)$$

$$+ \sum_{e \in \mathcal{E}_h} \int_e \frac{1}{2} |\mathbf{u}_h \cdot \mathbf{n}_e| \llbracket \rho_h \rrbracket \cdot \llbracket \zeta_h \rrbracket \, ds, \quad (18)$$

$$c_2^h(\rho_h \mathbf{w}_h; \mathbf{u}_h, \mathbf{v}_h) := \int_\Omega (\rho_h \mathbf{w}_h \cdot \nabla_h) \mathbf{u}_h \cdot \mathbf{v}_h \, dx + \frac{1}{2} \int_\Omega \nabla \cdot (\rho_h \mathbf{w}_h) \mathbf{u}_h \cdot \mathbf{v}_h \, dx \quad (19)$$

$$- \sum_{e \in \mathcal{E}_h} \int_e (\rho_h \mathbf{w}_h \cdot \mathbf{n}_e) \llbracket \mathbf{u}_h \rrbracket \cdot \{\{\mathbf{v}_h\}\} \, ds + \sum_{e \in \mathcal{E}_h} \int_e \frac{1}{2} |\rho_h \mathbf{w}_h \cdot \mathbf{n}_e| \llbracket \mathbf{u}_h \rrbracket \cdot \llbracket \mathbf{v}_h \rrbracket \, ds, \quad (20)$$

where $a_0 > 0$ is a jump penalization parameter. Further, \mathbf{z}_h is an auxiliary variable which help us to decouple the regularized part of the second equation in (5), and handle as a separate equation the variational version of the Huber equation (3), given by the last equation in (14). The introduction of this function has proven to be an efficient way to handle the non-linearity associated to the Huber regularization, as seen in [6, 13, 20].

3.3 Complete discrete scheme

We now define the approximate sequences $\{\rho_h^n\}_{n=0, \dots, N}$, $\{\mathbf{u}_h^n\}_{n=0, \dots, N}$, $\{p_h^n\}_{n=0, \dots, N}$ and $\{\mathbf{z}_h^n\}_{n=0, \dots, N}$ as follows: For $1 \leq n \leq N-1$, solve:

$$\begin{aligned} \frac{1}{2\Delta t} (\mathcal{D} \rho_h^{n+1}, \zeta_h)_\Omega + c_1^h(\mathbf{u}_h^{n+1}, \rho_h^{n+1}, \zeta_h) &= 0, \\ \frac{1}{2\Delta t} (\sigma_h^{n+1} \mathcal{D}_h(\sigma_h^{n+1} \mathbf{u}_h^{n+1}), \mathbf{v}_h)_\Omega + a_2^h(\mathbf{u}_h^{n+1}, \mathbf{v}_h) + (\mathbf{z}_h^{n+1}, \mathbf{D}_h \mathbf{v}_h)_\Omega \\ + c_2^h(\rho_h^{n+1} \mathbf{u}_h^{n+1}; \mathbf{u}_h^{n+1}, \mathbf{v}_h) + b(p_h^{n+1}, \mathbf{v}_h) &= (\mathbf{f}^{n+1}, \mathbf{v}_h)_\Omega, \\ b(q_h, \mathbf{u}_h^{n+1}) &= 0, \\ (\gamma \tau_s \mathbf{D}_h \mathbf{u}_h^{n+1}, \mathbf{w}_h)_\Omega - (|\mathbf{D}_h \mathbf{u}_h^{n+1}|_\gamma \mathbf{z}_h^{n+1}, \mathbf{w}_h)_\Omega &= 0. \end{aligned} \quad (21)$$

for all $\zeta_h \in \mathcal{W}_h$, $\mathbf{v}_h \in \mathbf{V}_h$, $q_h \in \mathcal{Q}_h$ and $\mathbf{w}_h \in \mathbf{W}_h$.

3.4 Stability analysis of the discrete scheme

For the subsequent analysis, we introduce, for $r \geq 0$, the broken \mathbf{H}^r space as follows.

$$\mathbf{H}^r(\mathcal{T}_h) := \{\mathbf{v} \in \mathbf{L}^2(\Omega) : \mathbf{v}|_K \in \mathbf{H}^r(K), K \in \mathcal{T}_h\},$$

as well as the mesh-dependent broken norms

$$\begin{aligned} \|\mathbf{v}\|_{*,\mathcal{T}_h}^2 &:= \sum_{K \in \mathcal{T}_h} \|\mathbf{D}_h(\mathbf{v})\|_{0,K}^2 + \sum_{e \in \mathcal{E}_h} \frac{1}{h_e} \|\llbracket \mathbf{v} \rrbracket\|_{0,e}^2, \\ \|\mathbf{v}\|_{1,\mathcal{T}_h}^2 &:= \|\mathbf{v}\|_{0,\Omega}^2 + \|\mathbf{v}\|_{*,\mathcal{T}_h}^2 \quad \text{for all } \mathbf{v} \in \mathbf{H}^1(\mathcal{T}_h), \\ \|\mathbf{v}\|_{2,\mathcal{T}_h}^2 &:= \|\mathbf{v}\|_{1,\mathcal{T}_h}^2 + \sum_{K \in \mathcal{T}_h} h_K^2 |\mathbf{v}|_{2,K}^2 \quad \text{for all } \mathbf{v} \in \mathbf{H}^2(\mathcal{T}_h), \end{aligned}$$

where the stronger norm $\|\cdot\|_{2,\mathcal{T}_h}$ is used to show continuity. By using the inverse estimate

$$|\mathbf{w}|_{2,K} \leq Ch_K^{-1} |\mathbf{w}|_{1,K}, \quad \text{for all } K \in \mathcal{T}_h, \mathbf{w} \in [\mathbb{P}_k(K)]^d,$$

it can be seen that this norm is equivalent to $\|\cdot\|_{1,\mathcal{T}_h}$ on \mathbf{V}_h (see, e.g., [3]). We also define the discrete kernel of the bilinear form $b(\cdot, \cdot)$ as

$$\mathbf{K}_h := \{\mathbf{v}_h \in \mathbf{V}_h : b(\mathbf{v}_h, q_h) = 0 \forall q_h \in \mathcal{Q}_h\} = \{\mathbf{v}_h \in \mathbf{V}_h : \text{Div } \mathbf{v}_h = 0 \text{ in } \Omega\}. \quad (22)$$

Finally, adapting the argument used in [26, Proposition 4.5], we have the discrete Sobolev embedding: for $r = 2, 4$ there exists a constant $C_{\text{emb}} > 0$ such that

$$\|\mathbf{v}\|_{\mathbf{L}^r(\Omega)} \leq C_{\text{emb}} \|\mathbf{v}\|_{1,\mathcal{T}_h}, \quad \text{for all } \mathbf{v} \in \mathbf{H}^1(\mathcal{T}_h). \quad (23)$$

With these norms, we can establish continuity of the bilinear forms constituting the variational formulation. The proof follows from [3, Section 4].

Lemma 3.1. *The following properties hold:*

$$\begin{aligned} |a_2^h(\mathbf{u}, \mathbf{v})| &\leq C \|\mathbf{u}\|_{2,\mathcal{T}_h} \|\mathbf{v}\|_{1,\mathcal{T}_h}, & \text{for all } \mathbf{u} \in \mathbf{H}^2(\mathcal{T}_h), \mathbf{v} \in \mathbf{V}_h, \\ |a_2^h(\mathbf{u}, \mathbf{v})| &\leq \tilde{C}_a \|\mathbf{u}\|_{1,\mathcal{T}_h} \|\mathbf{v}\|_{1,\mathcal{T}_h}, & \text{for all } \mathbf{u}, \mathbf{v} \in \mathbf{V}_h, \\ |b(\mathbf{v}, q)| &\leq \tilde{C}_b \|\mathbf{v}\|_{1,\mathcal{T}_h} \|q\|_{0,\Omega}, & \text{for all } \mathbf{v} \in \mathbf{H}^1(\mathcal{T}_h), q \in L^2(\Omega). \end{aligned}$$

Furthermore the following property holds (cf. [27, Lemma 3.2])

$$a_2^h(\mathbf{v}, \mathbf{v}) \geq \tilde{\alpha}_a \|\mathbf{v}\|_{1,\mathcal{T}_h}^2 \quad \text{for all } \mathbf{v} \in \mathbf{V}_h, \quad (24)$$

provided that the stabilization parameter $a_0 > 0$ in (15) is sufficiently large and independent of the mesh size.

Let $\mathbf{w} \in \mathbf{H}_0(\text{Div}^0; \Omega)$ and let us introduce the following vector and scalar jump seminorms

$$\begin{aligned} |\mathbf{u}_h|_{\mathbf{w}, \text{upw}} &:= \sum_{e \in \mathcal{E}_h^i} \int_e \frac{1}{2} |\mathbf{w}_e \cdot \mathbf{n}_e| |\llbracket \mathbf{u}_h \rrbracket|^2 ds, \\ |\rho_h|_{\mathbf{w}, \text{upw}} &:= \sum_{e \in \mathcal{E}_h^i} \int_e \frac{1}{2} |\mathbf{w}_e \cdot \mathbf{n}_e| |\llbracket \rho_h \rrbracket|^2 ds. \end{aligned}$$

Then, due to the skew-symmetric form of the operators c_1^h and c_2^h , and the positivity of the non-linear upwind terms (see i.e [29] and [15, Section 2.3.1]), we can write

$$c_1^h(\mathbf{w}; \psi_h, \psi_h) = |\psi_h|_{\mathbf{w}, \text{upw}}^2 \geq 0 \quad \text{for all } \psi_h \in \mathcal{W}_h, \quad (25a)$$

$$c_2^h(\rho \mathbf{w}; \mathbf{u}, \mathbf{u}) = |\mathbf{u}|_{\rho \mathbf{w}, \text{upw}}^2 \geq 0 \quad \text{for all } \mathbf{u} \in \mathbf{V}_h. \quad (25b)$$

Finally, we recall from [27] the following discrete inf-sup condition for $b(\cdot, \cdot)$, where $\tilde{\beta}$ is independent of h :

$$\sup_{\mathbf{v}_h \in \mathbf{V}_h \setminus \{0\}} \frac{b(\mathbf{v}_h, q_h)}{\|\mathbf{v}_h\|_{1, \mathcal{T}_h}} \geq \tilde{\beta} \|q_h\|_{0, \Omega}, \quad \text{for all } q_h \in \mathcal{Q}_h. \quad (26)$$

Theorem 3.2. *Let $(\rho_h^{n+1}, \mathbf{u}_h^{n+1}, p_h^{n+1}, \mathbf{z}_h^{n+1}) \in \mathcal{W}_h \times \mathbf{V}_h \times \mathcal{Q}_h \times \mathbf{W}_h$ be a solution of problem (21), with initial data $(\rho_h^1, \mathbf{u}_h^1)$ and $(\rho_h^0, \mathbf{u}_h^0)$. Then the following bounds are satisfied, where C_1 and C_2 are constants that are independent of h and Δt :*

$$\begin{aligned} & \|\rho_h^{n+1}\|_{0, \Omega}^2 + \|2\rho_h^{n+1} - \rho_h^n\|_{0, \Omega}^2 + \sum_{j=1}^n \|\Lambda \rho_h^j\|_{0, \Omega}^2 + \sum_{j=1}^n \Delta t |\rho_h^{j+1}|_{\mathbf{u}_h^{j+1}, \text{upw}}^2 \\ & \leq C_1 (\|\rho_h^1\|_{0, \Omega}^2 + \|2\rho_h^1 - \rho_h^0\|_{0, \Omega}^2), \\ & \|\sigma_h^{n+1} \mathbf{u}_h^{n+1}\|_{0, \Omega}^2 + \|2\sigma_h^{n+1} \mathbf{u}_h^{n+1} - \sigma_h^n \mathbf{u}_h^n\|_{0, \Omega}^2 + \sum_{j=1}^n \|\Lambda \mathbf{u}_h^j\|_{0, \Omega}^2 + \sum_{j=1}^n \Delta t \|\mathbf{u}_h^{j+1}\|_{1, \mathcal{T}_h}^2 \\ & + \sum_{j=1}^n \Delta t |\mathbf{u}_h^j|_{\mathbf{u}_h^j, \text{upw}}^2 \leq C_2 (\|\mathbf{f}\|_{L^\infty(0, T, \mathbf{L}^2(\Omega))}^2 + \|\sigma_h^1 \mathbf{u}_h^1\|_{0, \Omega}^2 + \|2\sigma_h^1 \mathbf{u}_h^1 - \sigma_h^0 \mathbf{u}_h^0\|_{0, \Omega}^2). \end{aligned} \quad (27)$$

Proof. We will require the following algebraic relation: for any real positive numbers a^{n+1} , a^n , a^{n-1} and defining $\Lambda a^n := a^{n+1} - 2a^n + a^{n-1}$, we have

$$2(3a^{n+1} - 4a^n + a^{n-1}, a^n) = |a^{n+1}|^2 + |2a^{n+1} - a^n|^2 + |\Lambda a^n|^2 - |a^n|^2 - |2a^n - a^{n-1}|^2. \quad (28)$$

First we take $\zeta_h = 4\rho_h^{n+1}$ in the first equation of (21), multiply by Δt and apply (28) and (25a) to deduce the estimate

$$\|\rho_h^{n+1}\|_{0, \Omega}^2 + \|2\rho_h^{n+1} - \rho_h^n\|_{0, \Omega}^2 + \|\Lambda \rho_h^n\|_{0, \Omega}^2 + 4\Delta t |\rho_h^{n+1}|_{\mathbf{u}_h^{n+1}, \text{upw}}^2 \leq \|\rho_h^n\|_{0, \Omega}^2 + \|2\rho_h^n - \rho_h^{n-1}\|_{0, \Omega}^2.$$

Summing over n we can assert that

$$\|\rho_h^{n+1}\|_{0, \Omega}^2 + \|2\rho_h^{n+1} - \rho_h^n\|_{0, \Omega}^2 + \sum_{j=1}^n \|\Lambda \rho_h^j\|_{0, \Omega}^2 + \sum_{j=1}^n \Delta t |\rho_h^{j+1}|_{\mathbf{u}_h^{j+1}, \text{upw}}^2 \leq \|\rho_h^1\|_{0, \Omega}^2 + \|2\rho_h^1 - \rho_h^0\|_{0, \Omega}^2.$$

Now in the fourth equation of (21), we take $\mathbf{w}_h = \frac{\mathbf{D}_h \mathbf{u}_h^{n+1}}{|\mathbf{D}_h \mathbf{u}_h^{n+1}|_\gamma}$ (which is possible since $\mathbf{u}_h^{n+1} \in \mathbf{H}(\text{Div}; \Omega)$ and $\mathbf{D}_h \mathbf{u}_h^{n+1}|_K \in [\mathbb{P}^{k-1}(K)]^{d \times d}$), to deduce the inequality,

$$0 \leq \tau_s \gamma \int \frac{|\mathbf{D}_h \mathbf{u}_h^{n+1}|^2}{|\mathbf{D}_h \mathbf{u}_h^{n+1}|_\gamma} dx = (\mathbf{z}_h^{n+1}, \mathbf{D}_h \mathbf{u}_h^{n+1})_\Omega \quad (29)$$

Similarly in the second and third equation of (21), we take $\mathbf{V}_h = 4\mathbf{u}_h^{n+1}$ and $q_h = 4p_h^{n+1}$, respectively, multiply by Δt and apply (28), (24), (25b) and (29) to deduce the estimate

$$\begin{aligned} & \|\sigma_h^{n+1} \mathbf{u}_h^{n+1}\|_{0, \Omega}^2 + \|2\sigma_h^{n+1} \mathbf{u}_h^{n+1} - \sigma_h^n \mathbf{u}_h^n\|_{0, \Omega}^2 + \|\Lambda \sigma_h^n \mathbf{u}_h^n\|_{0, \Omega}^2 + 4\Delta t \tilde{\alpha}_a \|\mathbf{u}_h^{n+1}\|_{1, \mathcal{T}_h}^2 + 4\Delta t |\mathbf{u}_h^{n+1}|_{\mathbf{u}_h^{n+1}, \text{upw}}^2 \\ & \leq 4\Delta t \|\mathbf{f}^{n+1}\|_{0, \Omega} \|\mathbf{u}_h^{n+1}\|_{0, \Omega} + \|\mathbf{u}_h^n\|_{0, \Omega}^2 + \|2\mathbf{u}_h^n - \mathbf{u}_h^{n-1}\|_{0, \Omega}^2. \end{aligned}$$

Using Young's inequality with $\varepsilon = \tilde{\alpha}_a/2$ and summing over n we can assert that

$$\begin{aligned}
& \|\sigma_h^{n+1} \mathbf{u}_h^{n+1}\|_{0,\Omega}^2 + \|2\sigma_h^{n+1} \mathbf{u}_h^{n+1} - \sigma_h^n \mathbf{u}_h^n\|_{0,\Omega}^2 + \sum_{j=1}^n \|\Lambda \sigma_h^j \mathbf{u}_h^j\|_{0,\Omega}^2 \\
& + 2\tilde{\alpha}_a \sum_{j=1}^n \Delta t \|\mathbf{u}_h^{j+1}\|_{1,\mathcal{T}_h}^2 + \sum_{j=1}^n 4\Delta t |\mathbf{u}_h^{j+1}|_{\mathbf{u}_h^{j+1}, \text{upw}}^2 \\
& \leq C \|\mathbf{f}\|_{L^\infty(0,T,\mathbf{L}^2(\Omega))} + \|\sigma_h^1 \mathbf{u}_h^1\|_{0,\Omega}^2 + \|2\sigma_h^1 \mathbf{u}_h^1 - \sigma_h^0 \mathbf{u}_h^0\|_{0,\Omega}^2.
\end{aligned} \tag{30}$$

□

Theorem 3.3 (Existence of discrete solutions). *Problem (21) with initial data $(\rho_h^1, \mathbf{u}_h^1)$ and $(\rho_h^0, \mathbf{u}_h^0)$ admits at least one solution*

$$(\rho_h^{n+1}, \mathbf{u}_h^{n+1}, p_h^{n+1}, \mathbf{z}_h^{n+1}) \in \mathcal{W}_h \times \mathbf{V}_h \times \mathcal{Q}_h \times \mathbf{W}_h.$$

The proof of Theorem 3.3 makes use of Brouwer's fixed-point theorem in the following form (given by [18, Corollary 1.1, Chapter IV]):

Theorem 3.4 (Brouwer's fixed-point theorem). *Let H be a finite-dimensional Hilbert space with scalar product $(\cdot, \cdot)_H$ and corresponding norm $\|\cdot\|_H$. Let $\Phi: H \rightarrow H$ be a continuous mapping for which there exists $\mu > 0$ such that $(\Phi(u), u)_H \geq 0$ for all $u \in H$ with $\|u\|_H = \mu$. Then there exists $u \in H$ such that $\Phi(u) = 0$ and $\|u\|_H \leq \mu$.*

Proof of Theorem 3.3. To simplify the proof we introduce the constants

$$\begin{aligned}
C_\rho &:= C_1 (\|\rho_h^1\|_{0,\Omega}^2 + \|2\rho_h^1 - \rho_h^0\|_{0,\Omega}^2), \\
C_u &:= C_2 (\|\mathbf{f}\|_{L^\infty(0,T,\mathbf{L}^2(\Omega))}^2 + \|\sigma_h^1 \mathbf{u}_h^1\|_{0,\Omega}^2 + \|2\sigma_h^1 \mathbf{u}_h^1 - \sigma_h^0 \mathbf{u}_h^0\|_{0,\Omega}^2).
\end{aligned}$$

We proceed by induction on $n \geq 2$. We define the mapping

$$\Phi: \mathcal{W}_h \times \mathbf{V}_h \times \mathcal{Q}_h \times \mathbf{W}_h \rightarrow \mathcal{W}_h \times \mathbf{V}_h \times \mathcal{Q}_h \times \mathbf{W}_h, \tag{31}$$

using the relation

$$\begin{aligned}
& (\Phi(\rho_h^{n+1}, \mathbf{u}_h^{n+1}, p_h^{n+1}, \mathbf{z}_h^{n+1}), (\zeta_h, \mathbf{v}_h, q_h, \mathbf{w}_h))_\Omega \\
& = \frac{1}{2\Delta t} (\mathcal{D}\rho_h^{n+1}, \zeta_h)_\Omega + c_1^h(\mathbf{u}_h^{n+1}, \rho_h^{n+1}, \zeta_h) + \\
& \quad \frac{1}{2\Delta t} (\sigma_h^{n+1} \mathcal{D}_h(\sigma_h^{n+1} \mathbf{u}_h^{n+1}), \mathbf{v}_h)_\Omega + a_2^h(\mathbf{u}_h^{n+1}, \mathbf{v}_h) + (\mathbf{z}_h^{n+1}, \mathbf{D}_h \mathbf{v}_h)_\Omega \\
& \quad + c_2^h(\rho_h^{n+1} \mathbf{u}_h^{n+1}, \mathbf{u}_h^{n+1}, \mathbf{v}_h) + b(p_h^{n+1}, \mathbf{v}_h) - (\mathbf{f}^{n+1}, \mathbf{v}_h)_\Omega \\
& \quad - b(q_h, \mathbf{u}_h^{n+1}) - (\gamma \tau_s \mathbf{D}_h \mathbf{u}_h^{n+1}, \mathbf{w}_h)_\Omega + (|\mathbf{D}_h \mathbf{u}_h^{n+1}|_\gamma \mathbf{z}_h^{n+1}, \mathbf{w}_h)_\Omega.
\end{aligned}$$

Note that this map is well-defined and continuous on $\mathcal{W}_h \times \mathbf{V}_h \times \mathcal{Q}_h \times \mathbf{W}_h$. On the other hand, if we take

$$(\zeta_h, \mathbf{v}_h, q_h, \mathbf{w}_h) = \left(\rho_h^{n+1}, \mathbf{u}_h^{n+1}, p_h^{n+1}, \frac{1}{\gamma \tau_s} \mathbf{z}_h^{n+1} \right),$$

and employ (25a), (25b), (29) and (24), we obtain

$$\begin{aligned}
& \frac{1}{\gamma\tau_s} (\Phi(\rho_h^{n+1}, \mathbf{u}_h^{n+1}, p_h^{n+1}, \mathbf{z}_h^{n+1}), (\rho_h^{n+1}, \mathbf{u}_h^{n+1}, p_h^{n+1}, \mathbf{z}_h^{n+1}))_\Omega \\
& \geq \frac{3}{2\Delta t} \|\rho_h^{n+1}\|_{0,\Omega}^2 - \frac{1}{2\Delta t} (4\rho_h^n - \rho_h^{n-1}, \rho_h^{n+1})_\Omega + |\rho_h^{n+1}|_{\mathbf{u}_h^{n+1}, \text{upw}} \\
& + \frac{3}{2\Delta t} \|\mathbf{u}_h^{n+1}\|_{0,\Omega}^2 - \frac{1}{2\Delta t} (4\mathbf{u}_h^n - \mathbf{u}_h^{n-1}, \mathbf{u}_h^{n+1})_\Omega + \tilde{\alpha}_a \|\mathbf{u}_h^{n+1}\|_{1,\mathcal{T}_h}^2 \\
& + |\mathbf{u}_h^{n+1}|_{\mathbf{u}_h^{n+1}, \text{upw}}^2 - (\mathbf{f}^{n+1}, \mathbf{u}_h^{n+1})_\Omega.
\end{aligned}$$

Next, using (27) and Cauchy-Schwarz inequality, we deduce that

$$\begin{aligned}
& \frac{1}{\gamma\tau_s} (\Phi(\rho_h^{n+1}, \mathbf{u}_h^{n+1}, p_h^{n+1}, \mathbf{z}_h^{n+1}), (\rho_h^{n+1}, \mathbf{u}_h^{n+1}, p_h^{n+1}, \mathbf{z}_h^{n+1}))_\Omega \\
& \geq \frac{3}{2\Delta t} \|\rho_h^{n+1}\|_{0,\Omega}^2 - \frac{5}{2\Delta t} C_\rho \|\rho_h^{n+1}\|_{0,\Omega} \\
& \tilde{\alpha}_a \|\mathbf{u}_h^{n+1}\|_{0,\Omega}^2 - \|\mathbf{f}^{n+1}\|_{0,\Omega} \|\mathbf{u}_h^{n+1}\|_{0,\Omega}.
\end{aligned}$$

Then, setting

$$C_R = \gamma\tau_s \min \left\{ \frac{3}{2\Delta t}, \tilde{\alpha}_a \right\} \text{ and } C_r = \sqrt{2}\gamma\tau_s \max \left\{ \frac{5}{2\Delta t} C_\rho, \|\mathbf{f}\|_{L^\infty(0,T;\mathbf{L}^2(\Omega))} \right\},$$

we may apply the inequality $a + b \leq \sqrt{2}(a^2 + b^2)^{1/2}$, valid for all $a, b \in \mathbb{R}$, to obtain

$$\begin{aligned}
& (\Phi(\rho_h^{n+1}, \mathbf{u}_h^{n+1}, p_h^{n+1}, \mathbf{z}_h^{n+1}), (\rho_h^{n+1}, \mathbf{u}_h^{n+1}, p_h^{n+1}, \mathbf{z}_h^{n+1}))_\Omega \\
& \geq C_R (\|\rho_h^{n+1}\|_{0,\Omega}^2 + \|\mathbf{u}_h^{n+1}\|_{0,\Omega}^2) - C_r (\|\rho_h^{n+1}\|_{0,\Omega}^2 + \|\mathbf{u}_h^{n+1}\|_{0,\Omega}^2)^{1/2}.
\end{aligned}$$

Hence, the right-hand side is nonnegative on a sphere of radius $r := C_r/C_R$. Consequently, by Theorem 3.4, there exists a solution to the fixed-point problem $\Phi(\rho_h^{n+1}, \mathbf{u}_h^{n+1}, p_h^{n+1}, \mathbf{z}_h^{n+1}) = 0$, where the fixed-point map (31) is the solution operator for the fully discrete problem (21). \square

Note that, even when uniqueness of the discrete scheme remains an open problem, our non-exhaustive selection of numerical examples did not present any difficulties in this regard.

3.5 Semismooth Newton Linearization

At each time iteration we are left with a nonlinear system, which involves the non differentiable function associated to the Huber regularization $|\cdot|_\gamma$. This fact prevents us for proposing a Newton iteration to solve such a system. Despite this drawback, our goal remains to have a fast convergence method to solve this system. Thus, we propose a semismooth Newton (SSN) iteration, which lies in the use of the Newton or slantly differentiation. In the sake of readedness of the paper, we write this definition.

Definition 3.5. *Let X and Y be two Banach spaces, and let $D \subset X$ be an open domain. A function $F : D \subset X \rightarrow Y$ is said to be slantly differentiable at $x \in D$ if there exists a mapping $G_F : D \rightarrow \mathcal{L}(X, Y)$ such that the family $\{G_F(x + h)\}$ of bounded linear operators is uniformly bounded in the operator norm for h sufficiently small and*

$$\lim_{h \rightarrow 0} \frac{F(x + h) - F(x) - G_F(x + h)h}{\|h\|} = 0.$$

The use of this differentiation concept is justified, since it is well known that both the max function and the Frobenius norm are slantly differentiable in finite dimension spaces (see [13, 20, 21]). Further, the SSN approach has proved to be efficient and provided a linearization scheme which is superlinear convergent when applied to discretized viscoplastic models, as discussed in the referred contributions.

Given the discussion above, the SSN linearization for system (21), about $(\rho_h^{n+1}, \mathbf{u}_h^{n+1}, p_h^{n+1}, \mathbf{z}_h^{n+1})$, gives the following problem: find $\delta_\rho \in \mathcal{W}_h$, $\delta_{\mathbf{u}} \in \mathbf{V}_h$, $\delta_p \in \mathcal{Q}_h$, $\delta_{\mathbf{z}} \in \mathbf{W}_h$, such that, for all $\zeta_h \in \mathcal{W}_h$, $\mathbf{v}_h \in \mathbf{V}_h$, $q_h \in \mathcal{Q}_h$ and $\mathbf{w}_h \in \mathbf{W}_h$, we obtain the following system

$$\frac{3}{2\Delta t} \int_{\Omega} \delta_\rho \zeta_h \, dx + c_{1,\delta}^h(\mathbf{u}_h^{n+1}, \delta_{\mathbf{u}}, \rho_h^{n+1}, \delta_\rho, \zeta_h) = -\frac{1}{2\Delta t} \int_{\Omega} (\mathcal{D}\rho_h^{n+1} \zeta_h) \, dx - c_1^h(\mathbf{u}_h^{n+1}, \rho_h^{n+1}, \zeta_h) \quad (32a)$$

$$\begin{aligned} \frac{3}{2\Delta t} \int_{\Omega} ((\rho_h^{n+1} \delta_{\mathbf{u}} + \delta_\rho \mathbf{u}_h^{n+1}) \cdot \mathbf{v}_h) \, dx + a_2^h(\delta_{\mathbf{u}}, \mathbf{v}_h) + \int_{\Omega} (\delta_{\mathbf{z}} : \mathbf{D}_h \mathbf{v}_h) \, dx + b(\delta_p, \mathbf{v}_h) \\ + c_{2,\delta}^h(\rho_h^{n+1}, \delta_\rho, \mathbf{u}_h^{n+1}, \delta_{\mathbf{u}}; \mathbf{u}_h^{n+1}, \delta_{\mathbf{u}}, \mathbf{v}_h) = -\frac{1}{2\Delta t} \int_{\Omega} (\sigma_h^{n+1} \mathcal{D}(\sigma_h^{n+1} \mathbf{u}_h^{n+1}) \cdot \mathbf{v}_h) \, dx \\ - a_2^h(\mathbf{u}_h^{n+1}, \mathbf{v}_h) - \int_{\Omega} (\mathbf{z}_h^{n+1} : \mathbf{D}_h \mathbf{v}_h) \, dx - c_2^h(\rho_h^{n+1} \mathbf{u}_h^{n+1}; \mathbf{u}_h^{n+1}, \mathbf{v}_h) \\ - b(p_h^{n+1}, \mathbf{v}_h) + \int_{\Omega} \mathbf{f}^{n+1} \cdot \mathbf{v}_h \, dx, \end{aligned} \quad (32b)$$

$$b(q_h, \delta_{\mathbf{u}}) = -b(q_h, \mathbf{u}_h^{n+1}), \quad (32c)$$

$$\begin{aligned} \gamma \tau_s \int_{\Omega} \mathbf{D}_h \delta_{\mathbf{u}} : \mathbf{w}_h \, dx - \gamma \int_{\Omega} \frac{\chi_{\mathcal{A}_\gamma}}{|\mathbf{D}_h \mathbf{u}_h^{k+1}|} (\mathbf{D}_h \mathbf{u}_h^{k+1} : \mathbf{D}_h \delta_{\mathbf{u}}) (\mathbf{z}_h^{k+1} : \mathbf{w}_h) \, dx \\ - \int_{\Omega} |\mathbf{D}_h \mathbf{u}_h^{k+1}|_\gamma \delta_{\mathbf{z}} : \mathbf{w}_h \, dx = -\gamma \tau_s \int_{\Omega} \mathbf{D}_h \mathbf{u}_h^{k+1} : \mathbf{w}_h \, dx + \int_{\Omega} |\mathbf{D}_h \mathbf{u}_h^{k+1}|_\gamma \mathbf{z}_h^{k+1} : \mathbf{w}_h \, dx, \end{aligned} \quad (32d)$$

Let us discuss the equation (32d), associated with the Huber term $|\cdot|_\gamma$. Here, we have that

$$\chi_{\mathcal{A}_\gamma} := \begin{cases} 1, & \text{if } |\mathbf{D}_h \mathbf{u}_h| \geq \frac{\tau_s}{\gamma} \\ 0, & \text{otherwise.} \end{cases}$$

This function stands for the slantly derivative of the max term in $|\cdot|_\gamma$, and gives us a good estimator of the approximated yielded and unyielded regions in the material, respectively. In fact, the regions in which $\chi_{\mathcal{A}_\gamma} = 1$ are the active sets in the smoothing step and corresponds to the Huber approximations of the yielded regions. Respectively, the regions where $\chi_{\mathcal{A}_\gamma} = 0$, are the inactive sets and corresponds to the Huber approximations of the unyielded regions.

Next, let us focus on the convective forms $c_1^h(\mathbf{u}_h, \rho_h, \zeta_h)$ and $c_2^h(\rho_h \mathbf{w}_h, \mathbf{u}_h, \mathbf{v}_h)$. This forms are well posed due to the dG formulation and the analysis done in Section 3.4. In consequence, they are differentiable with derivatives given by $c_{1,\delta}^h(\mathbf{u}_h, \rho_h, \zeta_h)$ and $c_{2,\delta}^h(\rho_h \mathbf{w}_h, \mathbf{u}_h, \mathbf{v}_h)$

$$\begin{aligned} c_{1,\delta}^h(\mathbf{u}_h, \delta_{\mathbf{u}}; \rho_h, \delta_\rho, \zeta_h) &:= \int_{\Omega} (\mathbf{u}_h \cdot \nabla \delta_\rho + \delta_{\mathbf{u}} \cdot \nabla \rho_h) \zeta_h \, dx \\ &- \sum_{e \in \mathcal{E}_h} \int_e ((\delta_{\mathbf{u}} \cdot \mathbf{n}_e) \llbracket \rho_h \rrbracket + (\mathbf{u}_h \cdot \mathbf{n}_e) \llbracket \delta_\rho \rrbracket) \{\{\zeta_h\}\} \, ds \\ &+ \sum_{e \in \mathcal{E}_h} \int_e \frac{1}{2} \frac{\mathbf{u}_h \cdot \mathbf{n}_e}{|\mathbf{u}_h \cdot \mathbf{n}_e|} (\delta_{\mathbf{u}} \cdot \mathbf{n}_e) \llbracket \rho_h \rrbracket \cdot \llbracket \zeta_h \rrbracket \, ds \\ &+ \sum_{e \in \mathcal{E}_h} \int_e \frac{1}{2} |\mathbf{u}_h \cdot \mathbf{n}_e| \llbracket \delta_\rho \rrbracket \cdot \llbracket \zeta_h \rrbracket \, ds \end{aligned}$$

and

$$\begin{aligned}
c_{2,\delta}^h(\rho_h, \delta_\rho, \mathbf{w}_h, \delta_{\mathbf{w}}; \mathbf{u}_h, \delta_{\mathbf{u}}, \mathbf{v}_h) &:= \int_{\Omega} ((\rho_h \delta_{\mathbf{w}} + \delta_\rho \mathbf{w}_h) \cdot \nabla_h) \mathbf{u}_h \cdot \mathbf{v}_h \, dx + \int_{\Omega} (\rho_h \mathbf{w}_h \cdot \nabla_h) \delta_{\mathbf{u}} \cdot \mathbf{v}_h \, dx \\
&+ \frac{1}{2} \int_{\Omega} (\nabla \cdot (\delta_\rho \mathbf{w}_h + \rho_h \delta_{\mathbf{w}}) \mathbf{u}_h + \nabla \cdot (\rho_h \mathbf{w}_h) \delta_{\mathbf{u}}) \cdot \mathbf{v}_h \, dx \\
&- \sum_{e \in \mathcal{E}_h} \int_e ((\delta_\rho \mathbf{w}_h + \rho_h \delta_{\mathbf{w}}) \cdot \mathbf{n}_e) \llbracket \mathbf{u}_h \rrbracket + (\rho_h \mathbf{w}_h \cdot \mathbf{n}_e) \llbracket \delta_{\mathbf{u}} \rrbracket \cdot \{\{\mathbf{v}_h\}\} \, ds \\
&+ \sum_{e \in \mathcal{E}_h} \int_e \left(\frac{1}{2} |\rho_h \mathbf{w}_h \cdot \mathbf{n}_e| \llbracket \delta_{\mathbf{u}} \rrbracket + \frac{1}{2} \frac{\rho_h \mathbf{w}_h \cdot \mathbf{n}_e}{|\rho_h \mathbf{w}_h \cdot \mathbf{n}_e|} (\delta_\rho \mathbf{w}_h + \rho_h \delta_{\mathbf{w}}) \cdot \mathbf{n}_e \llbracket \mathbf{u}_h \rrbracket \right) \cdot \llbracket \mathbf{v}_h \rrbracket \, ds.
\end{aligned}$$

Summarizing, we can conclude that system (32) is well-posed (see [21] for further details). Moreover, by following a similar analysis as the one in [13] we can state that the SSN iteration converges superlinearly locally. This assertion will be computationally confirmed in the numerical experiments that are carried out in the next section.

4 Numerical results

In this section we test the performance of the numerical method on a set of quasi-uniform triangulations of the respective domain. The implementation of the $\mathbf{H}(\text{div})$ -conforming finite element scheme is carried out using the open source finite element library FEniCS [2] and polynomial degree $k = 1$. The linear systems encountered at each Newton-Raphson step are solved with the multi-frontal massively parallel sparse direct solver MUMPS. The Newton iterations stop whenever either the absolute or the relative residuals (measured in the ℓ_2 -norm) drop below the fixed tolerance set to 1×10^{-5} .

4.1 Viscous Rayleigh-Taylor Instability

As a test case we deal with a physically interesting problem the development of a Rayleigh–Taylor instability in the viscous regime. The problem has been studied in [17, 9], taking as starting point the work by Tryggvason [33]. We consider a domain $\Omega =]-l/2, l/2[\times]-2l, 2l[$ filled with two layers of fluid with varying density, initially at rest and subject to gravity. As proposed in [33], the interface at time $t = 0$, is given as follows:

$$\rho_0(x, y) = \frac{\rho_m + \rho_M}{2} + \frac{\rho_m - \rho_M}{2} \tanh \left(\frac{y - \eta \cos(2\pi x/l)}{0.01l} \right)$$

where $\rho_M > \rho_m > 0$ and $\eta > 0$ is the amplitude of the initial perturbation.

Defining as l the representative length of the column; we define dimensionless variables as

$$\tilde{\rho} = \frac{\rho}{\rho_m}, \quad \tilde{\mathbf{x}} = \frac{\mathbf{x}}{l}, \quad \tilde{t} = \frac{t}{l^{1/2} g^{-1/2}}, \quad \tilde{\mathbf{u}} = \frac{\mathbf{u}}{l^{1/2} g^{1/2}},$$

and we also define the following dimensionless numbers: The density ratio is measured by the Atwood number,

$$\text{At} = \frac{\rho_M - \rho_m}{\rho_M + \rho_m},$$

and the Reynolds number is defined as

$$\text{Re} = \frac{\rho_m l^{3/2} g^{1/2}}{\mu}$$

where $\mu > 0$ is the dynamic viscosity of the fluid and g is the gravitational acceleration. We take $\mathbf{f} = \rho \mathbf{g}$, with $\mathbf{g} = (0, -g)$. Furthermore, when presenting our numerical results for this example, we will use the time scale of Tryggvason (we have $t_{Try} = \tilde{t}\sqrt{At}$).

Making abuse of notation, in what follows, we will write it simply ρ , \mathbf{x} , t and \mathbf{u} , instead of $\tilde{\rho}$, $\tilde{\mathbf{x}}$, \tilde{t} and $\tilde{\mathbf{u}}$, respectively, when no confusion can arise.

Taking advantage of the fact that the solution has symmetries, as in [9], we compute the solution on the half domain $(0, l/2) \times (-2l, 2l)$ with the following boundary conditions for the velocity field: $\mathbf{u} = \mathbf{0}$ on the horizontal boundaries, and $\mathbf{u} = (0, v)$ with $\nabla \mathbf{u} \cdot \mathbf{n} = 0$ on the vertical boundaries.

As a sanity check, we start by analyzing the case with plasticity threshold close to zero ($\tau_s = 1 \times 10^{-3}$), in order to compare our qualitative results with previous works on Navier-Stokes variable density incompressible flows. Setting $At = 0.5$, (i.e. $\rho_M = 3$, $\rho_m = 1$) and initial condition $\eta = 0.1$, we simulate a low Reynolds case, $Re = 1000$, using a mesh of 60×100 cells. Comparing our qualitative results displayed in Figure 1, with those presented in [9, 17], there is a satisfactory agreement of the global characteristics of the flow in the early stages with some slight differences only at large times.

In figure 2, we also test the same setting with different mesh sizes: 60×100 (24000 cells), 120×200 (96000 cells) and 240×400 (384000). The solutions again, largely agree between them and the main features of the solution are still present in the coarser mesh.

The influence of the viscosity threshold τ_s is displayed on figure 3 where the rising counter-rotating vortices, develop slower as the viscosity thresholds increase its value. As expected the active set (\mathcal{A}_γ) also decreases. In fact, at the final tested value $\tau_s = 1.0$, there is not development of the vortices at time $t = 2.5$, with a change of the density interface almost imperceptible. Moreover, we can appreciate only a slight active zone around this interface.

Relative error for each SSN iteration is displayed in figure 4, for the $At = 0.5$ setting and $\tau_s = 1.0$, as can be seen, the convergence is slower for the first two time iterations (the backward Euler step and the first BDF2 approximation), clearly fast convergence is achieved as the initial approximation for the SSN iterations improves.

Now, we consider two Reynolds numbers, $Re = 1000$ and $Re = 5000$ for a high Atwood number problem. We set, $\rho_m = 1$ and $\rho_M = 9$, with initial condition $\eta = 0.01$, and relatively low $\tau_s = 0.1$. The results displayed in Figure 5, show a similar behavior to what was described for Newtonian fluids simulations (i.e. [9, 17]), the roll up of the heavy fluid is less pronounced, compared to those computed at low Atwood number and comparing the interface evolution for $Re = 1000$ and $Re = 5000$, it is clear that the viscosity plays no role on the downward motion velocity of the heavy fluid [9]. However, in general, rotating vortices are less developed, due to the plasticity threshold influence on the fluid dynamics, than what has been reported for the Newtonian counterparts of these tests.

4.2 Falling droplet

Now we investigate a droplet falling through a light fluid. The computational domain is $\Omega =]0, 0[\times]l, 1.5l[$, with $l = 2$. At time $t = 0$ the fluid is at rest with initial density given by

$$\rho(x, y) = \begin{cases} 15.0 & \text{if } 0 \leq \sqrt{(x - 1.0)^2 + (y - 2.75)^2} \leq 0.1 \\ 1.0 & \text{elsewhere} \end{cases}$$

The equations are made dimensionless by using the same reference quantities of the previous example. In our test we use nonslip boundary conditions in all walls, and a mesh of 40×60 cells. We set $Re = 1000$, and test two cases: zero plasticity threshold ($\tau_s = 0$), and $\tau_s = 1.0$. The qualitative

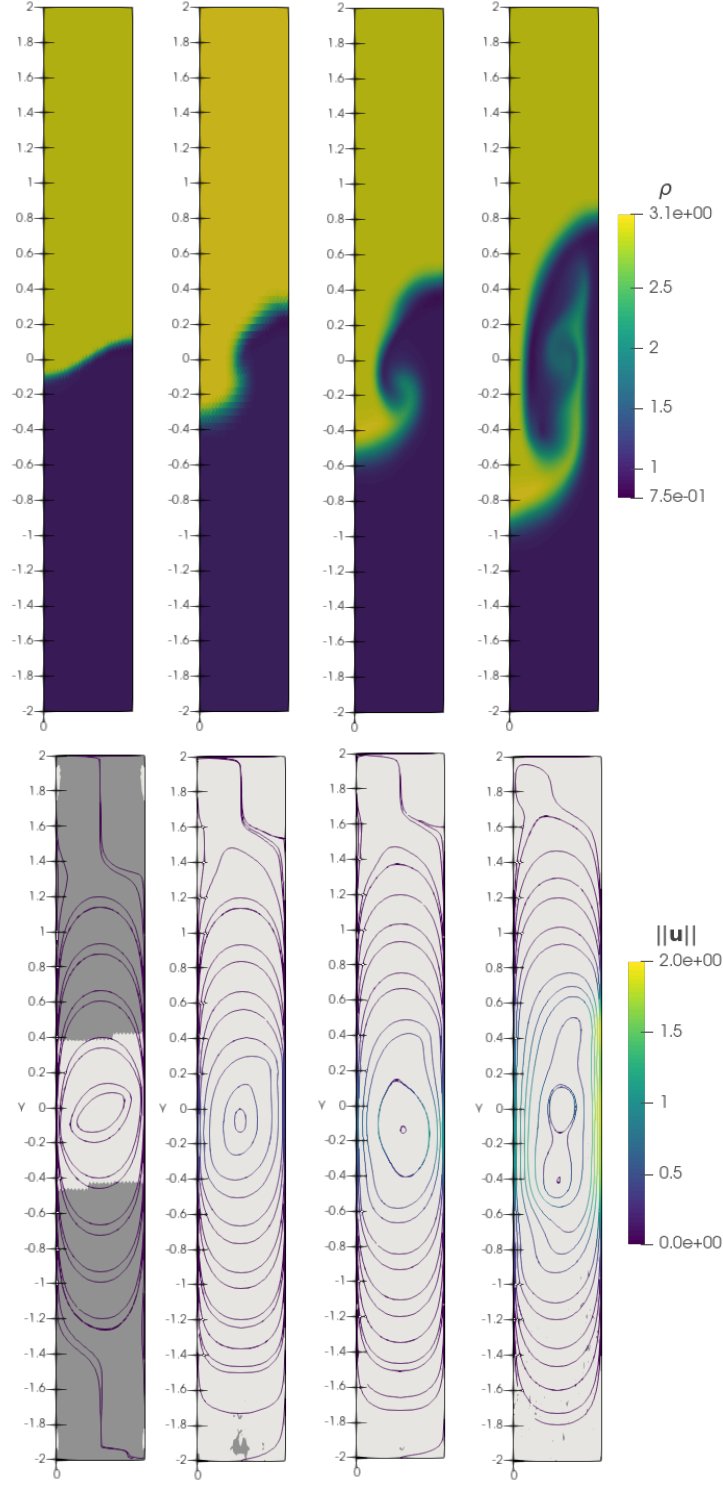


Figure 1: Rayleigh-Taylor instability. Top: Evolution of the density interface. Bottom: Velocity vector field stream lines and inactive set (dark gray). Times: 0.0, 1.0, 1.5 and 2.5 (from left to right). Parameters: $\tau_s = 1 \times 10^{-3}$, $\text{Re} = 1000$, $\eta = 0.1$

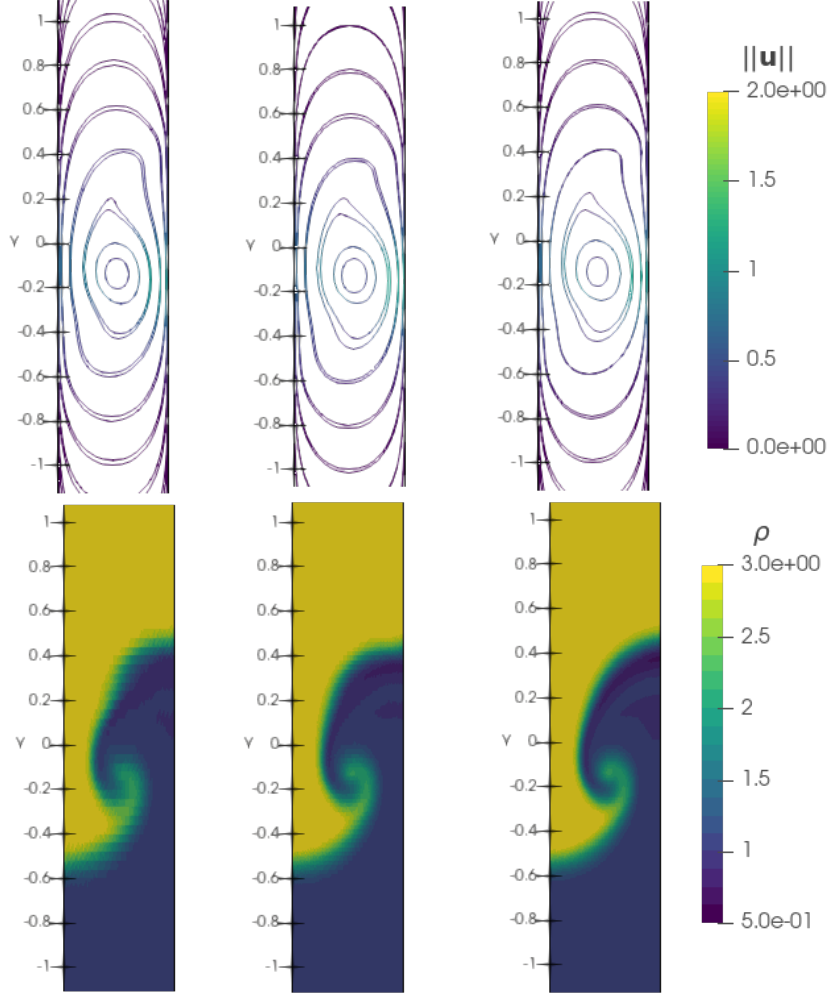


Figure 2: Rayleigh-Taylor instability. Velocity stream lines and density interface at time $t = 1.5$ for 24000, 96000 and 384000 cells. Parameters: $\tau_s = 1 \times 10^{-3}$, $\text{Re} = 1000$, $\eta = 0.1$

results are displayed in Figures 6 and 7. As we increase the τ_s value, the re-circulation patterns around the downwards droplet's path appear early, causing the split by half of the droplet. In fact, while in the zero threshold case the split occurs once the droplet reaches the domain bottom, in the $\tau_s = 1.0$ case the split starts as early as $t = 2.0$ snapshot. A closer look at the threshold plasticity $\tau_s = 1.0$ case, shows how the active zone moves following the droplet. Moreover, at time $t = 4$, additional stagnation zones start to form in the vortices center and the space between them (see Figure 7).

5 Conclusions

In this work, we have presented a second order divergence-conforming-dG method to the case of Bingham flows with non-uniform density. The scheme is based on a discontinuous Galerkin formulation for the mass density equation, stabilized with an upwind term, coupled with a divergence-conforming approximation of a Huber type regularization of the Bingham flow equation and using a BDF2 scheme for the time integration of the mass conservation and momentum equations. In

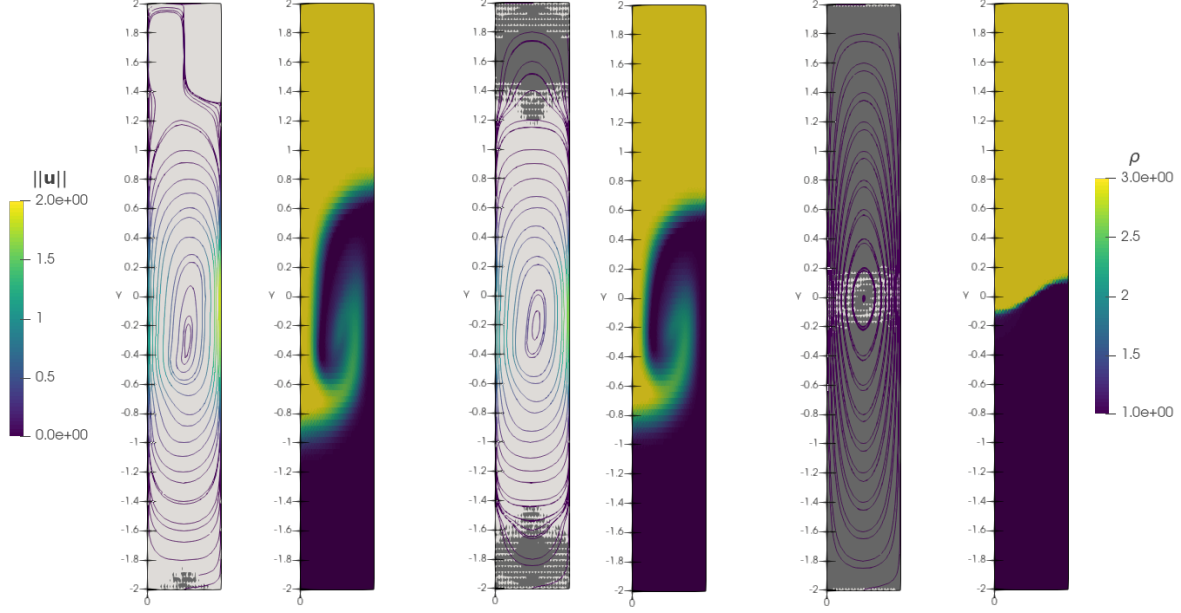


Figure 3: Rayleigh-Taylor instability. Velocity stream lines and inactive set (\mathcal{I}_γ , dark gray); and density interface at time $t = 2.5$ for $\tau_s = 1 \times 10^{-2}$, $\tau_s = 1 \times 10^{-1}$ and $\tau_s = 1.0$. Parameters: $\text{Re} = 1000$, $\eta = 0.1$

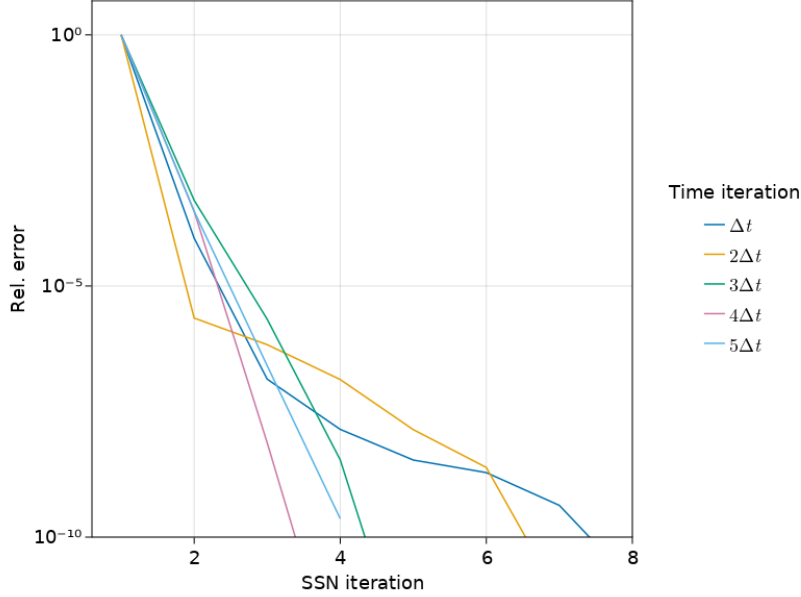


Figure 4: Rayleigh-Taylor instability: Relative Error vs SSN iterations for the first five time iterations. Parameters: $\tau_s = 1.0$, $\eta = 0.1$, $\Delta_t = 0.1$

each time step the space discretization resulting system is solved using a Semismooth Newton Iteration. We have proved the stability of the continuous problem, and the stability of the full-discrete scheme. To verify the correctness of the method, we compare our qualitative results with

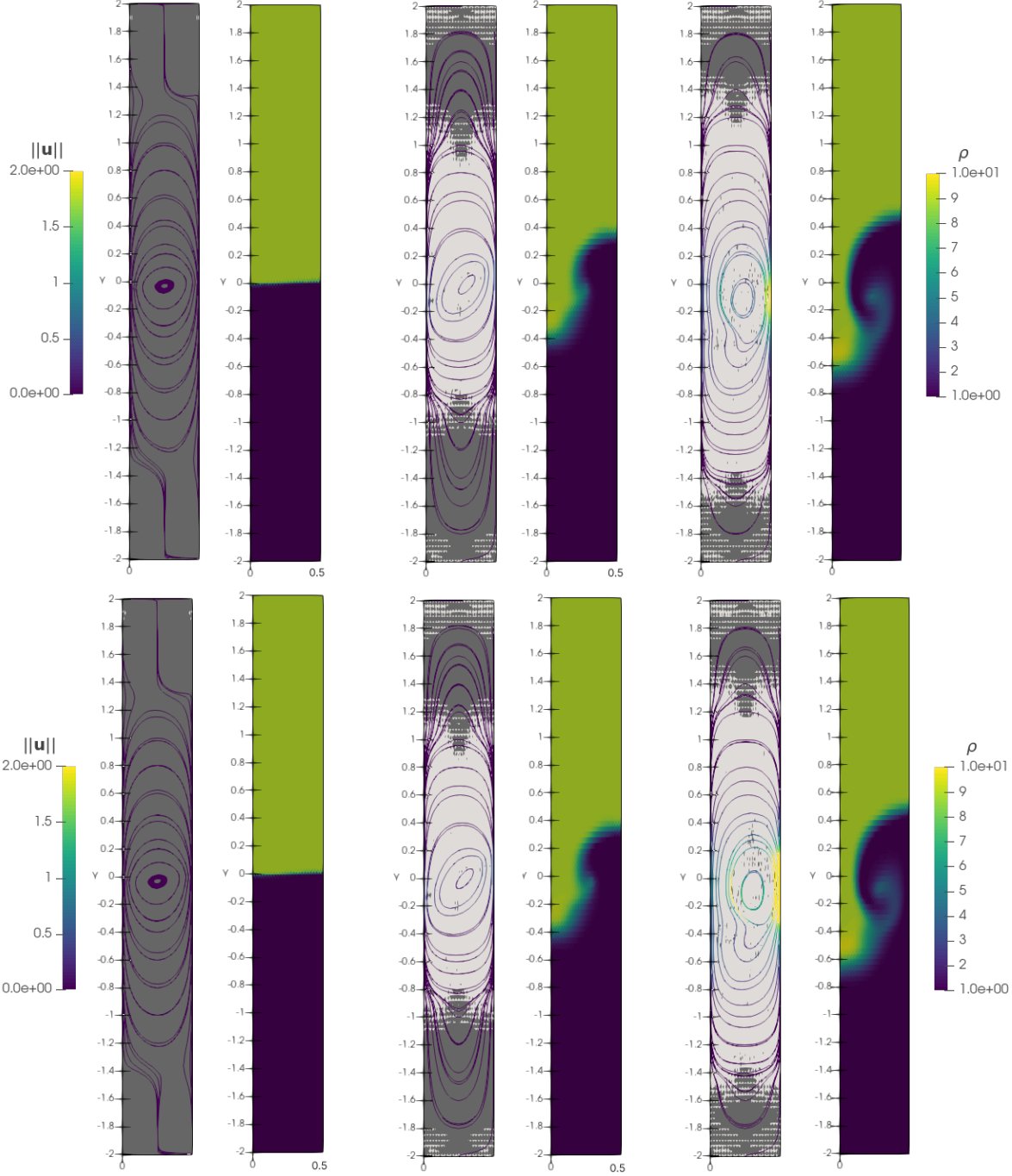


Figure 5: Rayleigh-Taylor instability. Velocity stream lines and inactive set (\mathcal{I}_γ , dark gray); and density interface at times $t = 0.0, 2.5$ and 3.0 for $Re=1000$ (top) and $Re=5000$ (bottom). Parameters: $\tau_s = 0.1, \eta = 0.01$

test cases previously considered in the literature. For instance when simulating the evolution of the Rayleigh–Taylor instability of the interface between fluids of different densities, the results of the method with low yield stress threshold are in agreement with the non-homogeneous Navier-Stokes computations in [9, 17] specially in the early stages of vortex formation and roll-up. Furthermore,

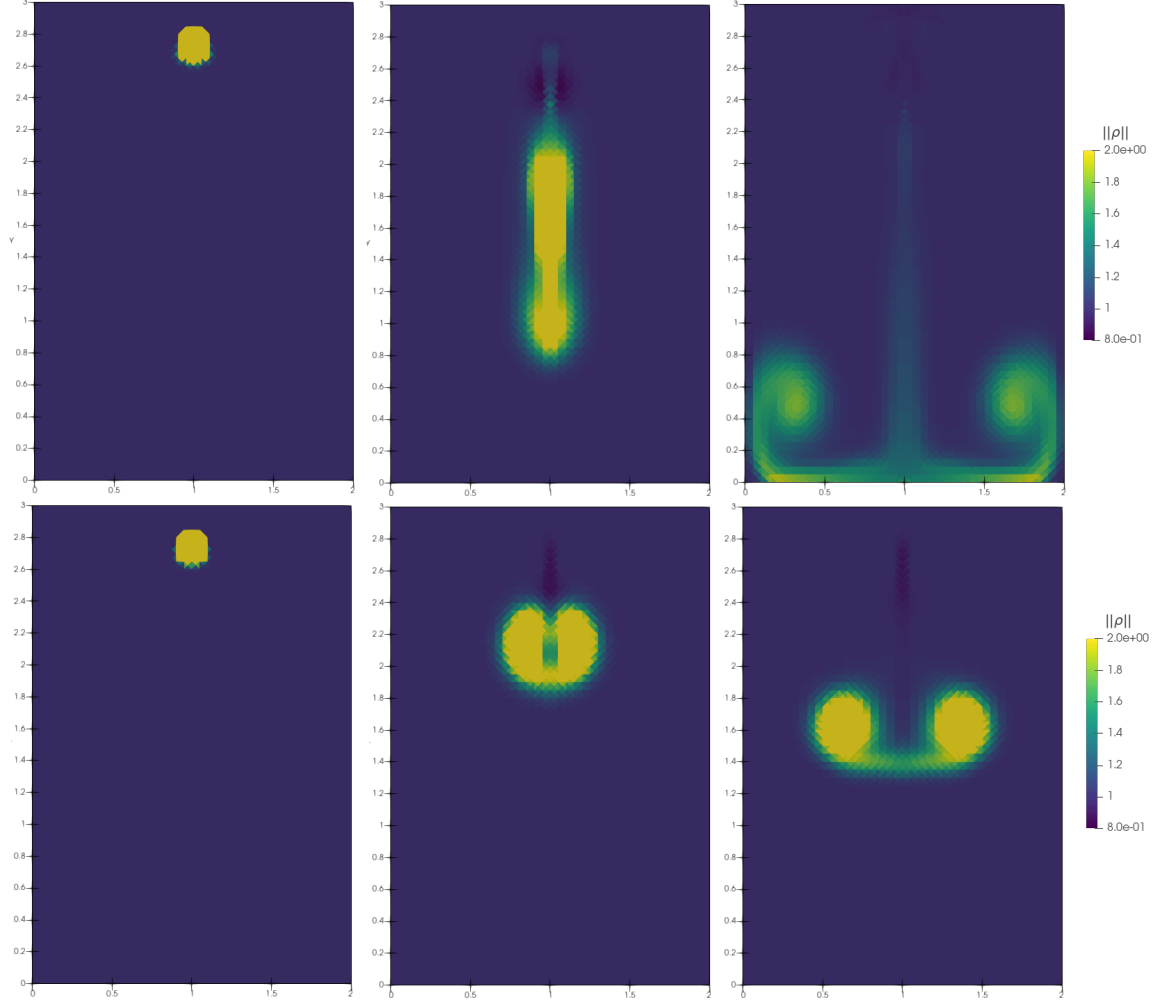


Figure 6: Falling Droplet: Density interface at times $t = 0.0, 2.0$ and 4.0 for $\tau_s = 0.0$ (top) and $\tau_s = 1.0$ (bottom). Parameters: $Re = 1000$

the simulations with different mesh refinements shows that even with rather coarser meshes we still can capture the main features of the density front.

Acknowledgement. We acknowledge the partial support by Escuela Politécnica Nacional del Ecuador, under the projects PIS 18-03 and PIGR 19-02. This research was carried out using the research computing facilities offered by Scientific Computing Laboratory of the Research Center on Mathematical Modeling: MODEMAT, Escuela Politécnica Nacional - Quito.

References

- [1] R. A. ADAMS, S.J.F FOURNIER, *Sobolev Spaces*, Academic Press, Elsevier, 4 ed. (2003)
- [2] M.S. Alnæs, J. Blechta, J. Hake, A. Johansson, B. Kehlet, A. Logg, C. Richardson, J. Ring, M.E. Rognes, G.N. Wells, *The FEniCS project version 1.5*, Archive of Numerical Software 3 (100) (2015) 9–23.

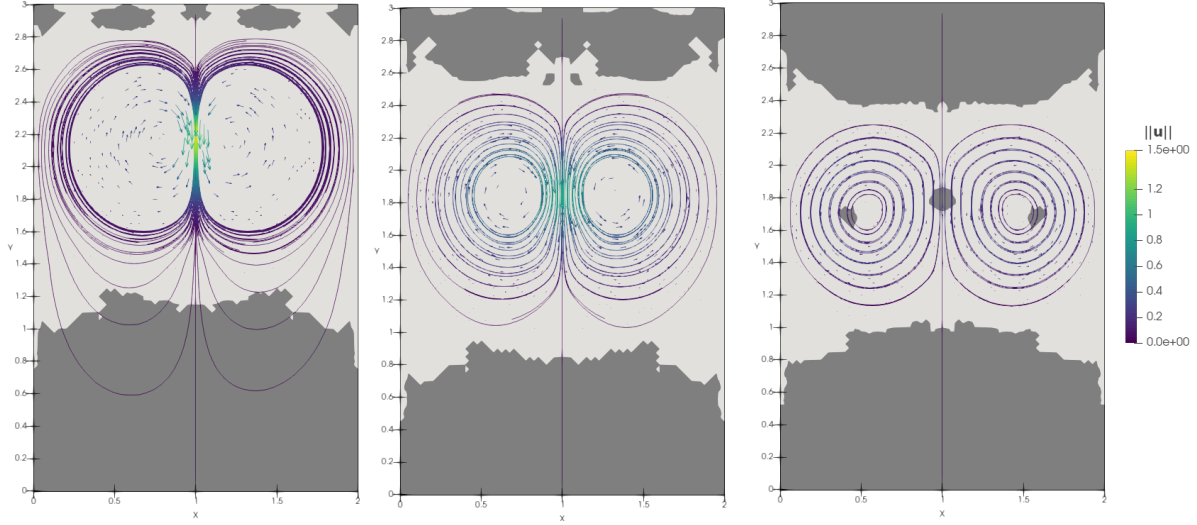


Figure 7: Falling Droplet. Velocity vector field stream lines and inactive set (\mathcal{I}_γ , dark gray); at times $t = 2.0, 3.0$ and 4.0 . Parameters: $\tau_s = 1.0$, $\text{Re} = 1000$

- [3] D.N. ARNOLD, F. BREZZI, B. COCKBURN, AND L.D. MARINI, *Unified analysis of discontinuous Galerkin methods for elliptic problems*. SIAM J. Numer. Anal., 39 (2002), pp. 1749–1779.
- [4] I. V. BASOV AND V. V. SHELUKHIN, *Nonhomogeneous incompressible Bingham viscoplastic as a limit of nonlinear fluids*, Journal of Non-Newtonian Fluid Mechanics, 142 (2007) 95–103.
- [5] S. CHEN AND V. BERTOLA. *Morphology of viscoplastic drop impact on viscoplastic surfaces*. SOFT MATTER, 13(2017), 711–719.
- [6] C.R. BEVERLY AND R. I. TANNER, *Numerical analysis of three-dimensional Bingham plastic flow*, Journal of non-Newtonian fluid mechanics, 42 (1992) 85 - 115.
- [7] M. BÖHM, *On a Nonhomogeneous Bingham Fluid*, Journal of Differential Equations, 60 (1985) 259–284.
- [8] F. BREZZI, J. DOUGLAS, L.D. MARINI, *Two families of mixed finite elements for second order elliptic problems*. Numer. Math. 47, (1985) 217–235.
- [9] C. CALGARO, E. CREUSÉ, AND T. *An hybrid finite volume-finite element method for variable density incompressible flows*. J. Comput. Phys. 227, 9 (2008), 4671–4696.
- [10] R. CHATELIN AND P. PONCET. *A parametric study of mucociliary transport by numerical simulations of 3D non-homogeneous mucus*. Journal of Biomechanics, 49(2016), 1772–1780.
- [11] B. COCKBURN, G. KANSCHAT, AND D. SCHÖTZAU. *A locally conservative LDG method for the incompressible Navier–Stokes equations*. Math. Comput., 74, (2005) 1067–1095.
- [12] R. DANCHIN. *Local and global well-posedness results for flows of inhomogeneous viscous fluids*. Adv. Differential Equations, 9(3-4), (2004), 353–386.
- [13] J. C. DE LOS REYES AND S. GONZÁLEZ ANDRADE, *A combined BDF-semismooth Newton approach for time-dependent Bingham flow*. Numerical Methods for Partial Differential Equations 28 (2012): 834–860.

- [14] A. YU DEMIANOV, A. N. DOLUDENKO, N. A. INOGAMOV AND E. E. SON. *Rayleigh–Taylor instability in a visco-plastic fluid*. Phys. Scr., 142 (2010) 014026
- [15] DI PIETRO, D.A., ERN, A., *Mathematical Aspects of Discontinuous Galerkin Methods. Mathématiques & Applications*. (Berlin) [Mathematics & Applications], vol. 69. Springer, Heidelberg (2012).
- [16] A. N. DOLUDENKO. *On contact instabilities of viscoplastic fluids in two-dimensional setting*. Computational Mathematics and Mathematical Physics, 57(2017), 1550–1557.
- [17] Y. FREIGNAUD., J.L. GUERMOND, L. QUARTAPELLE. *Approximation of variable density incompressible flows by means of finite elements and finite volumes*. Communications in Numerical Methods in Engineering 17 (2001): 893-902.
- [18] V. GIRAULT AND P.A. RAVIART, *Finite Element Methods for Navier-Stokes Equations. Theory and Algorithms*. Springer-Verlag, Berlin, 1986.
- [19] V. GIRAULT, B. RIVIÈRE, AND M.F. WHEELER, *A discontinuous Galerkin method with nonoverlapping domain decomposition for the Stokes and Navier-Stokes problems*. Math. Comput., 74 (2005), pp. 53–84.
- [20] S. GONZÁLEZ-ANDRADE, *A BDF2-Semismooth Newton Algorithm for the Numerical Solution of the Bingham Flow with Temperature Dependent Parameters*, Journal of Non-Newtonian Fluid Mechanics, 284 (2020) 104380.
- [21] S. GONZÁLEZ-ANDRADE AND P. E. MÉNDEZ, *A Dual-Mixed Approximation for a Huber Regularization of Generalized p -Stokes Viscoplastic Flow Problems*, arXiv:2104.04648.
- [22] J.-L. GUERMOND, L. QUARTAPELLE, *A Projection FEM for Variable Density Incompressible Flows*, Journal of Computational Physics, Volume 165, Issue 1 (2000), pp. 167-188,
- [23] J.-L. GUERMOND, A. SALGADO, *A splitting method for incompressible flows with variable density based on a pressure Poisson equation*, Journal of Computational Physics, Volume 228, Issue 8, (2009) 2834-2846.
- [24] P. HILD, I. R. IONESCU, T. LACHAND-ROBERT AND I. ROȘCA. *The Blocking of an Inhomogeneous Bingham Fluid. Applications to Landslides*. ESAIM:M2AN, 36 (2002) 1013–1026.
- [25] O. HUNGR. *Analysis of debris flow surges using the theory of uniformly progressive flow*. Earth Surf. Process. Landforms, 25 (2000) 483-495.
- [26] O.A. KARAKASHIAN AND W.N. JUREIDINI, *A nonconforming finite element method for the stationary Navier-Stokes equations*. SIAM J. Numer. Anal., 35 (1998), pp. 93–120.
- [27] J. KÖNNÖ AND R. STENBERG, *$H(\text{div})$ -conforming finite elements for the Brinkman problem*. Math. Models Methods Appl. Sci., 21 (2011), pp. 2227–2248.
- [28] C. LIU AND N.J. WALKINGTON, *Convergence of numerical approximations of the incompressible Navier–Stokes equations with variable density and viscosity*, SIAM J. Numer. Anal., 45 (2007) 1287–1304.
- [29] JAE-HONG PYO, JIE SHEN, *Gauge–Uzawa methods for incompressible flows with variable density*, Journal of Computational Physics, Volume 221, Issue 1 (2007), pp. 181-197

- [30] P.-L. LIONS, *Mathematical Topics in Fluid Mechanics: Volume 1: Incompressible Models*, Oxford Lecture Ser. Math. Appl. 3, The Clarendon Press, Oxford University Press, New York, (1996).
- [31] P.W. SCHROEDER, AND L. GERT. *Divergence-Free $H(\text{Div})$ -FEM for Time-Dependent Incompressible Flows with Applications to High Reynolds Number Vortex Dynamics*. Journal of Scientific Computing 75, no. 2 (2018): 830–58.
- [32] R. TEMAM, *Navier-Stokes equations. Theory and numerical analysis*. Reedition in the AMS-Chelsea Series, AMS, Providence, 2001.
- [33] G. TRYGGVASON. *Numerical simulations of the Rayleigh-Taylor instability*. J. Comput. Phys., (1988), 75:235–282.